Stimuli-induced non-equilibrium phase transitions in polyelectrolyte-surfactant complex coacervates

Chloé Seyrig, Gertrude Kignelman, Wim Thielemans, Patrick Le Griel, Nathan P Cowieson, Javier Perez, Niki Baccile

Published in Langmuir DOI: 10.1021/acs.langmuir.0c01177

Stimuli-induced non-equilibrium phase transitions in polyelectrolyte-surfactant complex coacervates

Chloé Seyrig,[a] Gertrude Kignelman,[b] Wim Thielemans,[b] Patrick Le Griel,[a] Nathan Cowieson,[c] Javier Perez,[d] Niki Baccile[a,*]

[a] Sorbonne Université, Centre National de la Recherche Scientifique, Laboratoire de Chimie de la Matière Condensée de Paris , LCMCP, F-75005 Paris, France

[b] Sustainable Materials Lab, Department of Chemical Engineering, KU Leuven, campus Kulak Kortrijk, Etienne Sabbelaan 53, 8500 Kortrijk, Belgium

[c] Diamond Light Source Ltd, Harwell Science and Innovation Campus, Didcot, OX11 0QX, U.K.

[d] SWING, Synchrotron Soleil, BP 48, 91192 Gif-sur-Yvette, France

* Corresponding author: niki.baccile@sorbonne-universite.fr

Abstract

Polyelectrolyte-surfactant complexes (PESCs) are important soft colloids with applications in the field of personal care, cosmetics, pharmaceutics and much more. If their phase diagrams have long been studied under pseudo-equilibrium conditions, and often inside the micellar or vesicular regions, understanding the effect of non-equilibrium conditions, applied at phase boundaries, on the structure of PESCs generates an increasing interest. In this work we cross the micelle-vesicle and micelle-fiber phase boundaries in an isocompositional surfactant-polyelectrolyte aqueous system through a continuous and rapid variation of pH. We employ two microbial glycolipid biosurfactants in the presence of polyamines, both systems being characterized by their responsiveness to pH. We show that complex coacervates (*Co*) are always formed in the micellar region of both glycolpids' phase diagram and that their phase behaviour drives the PESCs stability and structure. However, for glycolipid forming single-wall vesicles, we observe an isostructural and isodimensional transition between complex coacervates and a multilamellar walls vesicle (*MLWV*) phase. For the fiber-forming glycolipid, on the contrary, the complex coacervate disassembles into free polyelecrolyte coexisting with the equilibrium fiber phase. Last but not least, this work also demonstrates the use of microbial glycolipid biosurfactants in the development of sustainable PESCs.

Keywords. Polyelectrolyte-Surfactant Complex (PESC), complex coacervates, biosurfactants, polyelectrolytes, multilamellar walls vesicles

Introduction

Polyelectrolyte-surfactant complexes (PESCs) are a wide class of colloidal systems where surfactant's self-assembly is combined to the complexation properties of polyelectrolytes.[1–7] In the past three decades a large number of works has shown the interest of a wide community of scientists towards these systems for the broad set of applications in food science,[8] tissue engineering,[9] drug and gene delivery,[2,10] underwater adhesives conception,[11] structuring agents,[12] water treatment,[13] but also personal care, cosmetics,[14] food, pharmaceutical science[15–17] and much other.[5–7]

The structure of PESCs depend on many parameters, including the intrinsic packing parameter of the surfactant,[18] rigidity of the polyelectrolyte, charge density and distribution on both surfactant and polyelectrolyte, ionic strength and pH, just to cite the main ones.[3,4,6,7,19,20] Supramicellar aggregates are the most common structures when the surfactant is in the micellar region of its phase diagram. They can be found as polyelectrolyte-coated dense aggregates of spheroidal micelles, which can undergo either a solid-liquid,[3,7] or liquid-liquid,[3,21] phase separation. In the latter case, they are referred to as complex coacervates.[21,22] Supramicellar colloids can also be found in the form of pearl-necklace or cylindrical morphologies.[3,4] The micellar morphology and structure are generally not affected by complexation,[3,7,21,23] however, phase transitions can occur inside the supramicellar complexes due to the local rise in concentration.[3,4,7,24] Multilamellar PESCs, of both flat or vesicular morphologies, have also been explored from a fundamental point of view[3,5,7,19,25] for their interest in gene delivery applications, as described for DNA-complexed phospholipids, known as lipoplexes.[2,19]

Considering the importance of PESCs, the study of their phase diagrams started long ago for a wide range of surfactants complexed by polymers or block copolymers. The complexity of this task is high due to multidimensionality, where effects of ionic strength, cosolvent, cosurfactants and charge could be taken into account.[5,6,19,20,24–26] Even if the debate about whether PESCs are at equilibrium or not is still open,[3] the study of their phase diagram has long been addressed using a classical thermodynamic approach, involving a systematic parametric study and equilibration times. However, more recent trends consider the importance of crossing phase boundaries under non-equilibrium conditions.[3,4] This is motivated by both practical considerations on applications and fundamental questioning.[3] If non-equilibrium transitions are a recent concern in PESCs[3], they are in fact a major concern in the broader field

of macromolecular complexation,[27–29] and complex coacervation in particular, as shown by recent works, concerned by selective control of interactions between polyelectrolytes and lipids.[30,31] Molecular dynamics and diffusion-limited processes open again, under a new perspective, old questions such as possible shift of the surfactant's phase boundary, promotion of a new surfactant's phase but also PESC disassembling, promotion of a new PESC phase or coexistence between surfactant and polyelectrolyte phases.

The micelle-to-vesicle transition is particularly interesting because, while being classical in lyotropic surfactant and lipid phases,[25,32] it could be exploited in delivery applications under non-equilibrium conditions. Interestingly, non-equilibrium micelle-to-vesicle transitions are well-known,[33] however, to the best of our knowledge, they were rarely investigated in PESCs, even under pseudo-equilibrium conditions. The equilibrium phase diagram of ethoxy fatty acids in aqueous solutions displayed a pH-dependent micelle-to-vesicle transition,[34] but the same transition was not observed in the presence of polyelectrolytes,[35] thus confirming the yet unpredictable effect of polyelectrolytes on surfactants' phase diagram. This is particularly true in the case of lipid bilayer membranes, of which the physical properties, including the local composition, defects, segregation and bending energy depend on the polyion.[25,36–39] Even if the complexity of the interactions between polyelectrolytes and (soft) interfaces has been addressed for decades,[39–41] predicting the equilibrium curvature in PESCs[3] is still a challenge,[42,43] and this is a matter of utmost importance for more advanced applications of PESCs.[30,31]

Fibrillation of low-molecular weight compounds is also another important field of research, from both applicative (hydrogelation)[44] and fundamental (non-equilibrium phase transitions)[45] perspectives. Development of PESCs from low-molecular weight gelators is still a virgin field of research and questioning the interactions between polyelectrolytes and self-assembled fibers has only started with recent works.[46]

In a series of recent communications, many authors have addressed the solution self-assembly of microbial glycolipid biosurfactants.[47–49] These molecules have a multiple interest in the field of PESCs: they are biobased and biodegradable amphiphiles[50] with a rich phase diagram and stimuli responsiveness. For these reasons they are highly prompt for the development of biocompatible PESCs but also for the study of non-equilibrium phase transitions in complex systems, both aspects generating an increasing interest in the community.[3,7] In particular, we have shown that acidic C18:1 sophorolipids, which form a stable micellar phase in a broad pH range,[49,51,52] also form pH-responsive complex coacervates in the presence of both synthetic and natural polyamines.[53] Interestingly, sophorolipid

analogues have a richer, pH-stimulated, phase diagram including micelle-to-vesicle, micelle-to-fiber and micelle-to-lamellar transitions.[49,52,54]

In this work, we explore the stability of a polyelectrolyte-surfactant complex coacervate at two distinct iso-compositional phase boundaries, micelle-vesicle and micelle-fiber, where phase transition is triggered by pH. To do so, we use two microbial glycolipid biosurfactants in the presence of three cationic polyelectrolytes (PEC). Turbidimetric analysis, cryogenic transmission electron microscopy (cryo-TEM) and pH-resolved *in situ* small angle X-ray scattering (SAXS) using synchrotron radiation experiments show that complex coacervates are only stable in the micellar region of both glycolipids' phase diagram. However, if the lipid undergoes a micelle-to-vesicle transition, we observe a complex coacervate (*Co*) to multilamellar walls vesicles (*MLWV*) (*Co*-to-*MLWV*) phase transition. *MLWV* are composed of PEC entrapped between single lipid layers, of which the mutual interactions are quantified by nuclear magnetic resonance (NMR) and isothermal titration calorimetry (ITC). If the lipid undergoes a micelle-to-fiber transition, on the contrary, the coacervate disassembles and the glycolipid's fiber phase coexists with the polyelectrolyte, with no apparent interactions, against the literature's expectations.[46] Finally, this work demonstrates the use of biobased surfactants for the development of sustainable PESCs.

Experimental section

Chemicals

Glycolipids G-C18:1 (M_w= 460 g·mol^{-1}), made of a single *β*-D-glucose hydrophilic headgroup and a C18:1 fatty acid tail (monounsaturation in position 9,10), and SL-C18:0 (M_w= 624 g·mol^{-1}), composed of a sophorose headgroup and a stearic acid derivative. From alkaline to acidic pH, the former undergoes a micelle-to-vesicle phase transition[49] while the latter undergoes a micelle-to-fiber phase transition.[55] The syntheses of sophorolipid SL-C18:0 and glucolipid G-C18:1 are respectively described in Ref [55] and [54], where the typical ^{1}H NMR spectra and HPLC chromatograms are also given. The compounds used in this work have a molecular purity of more than 95%.

The cationic polyelectrolytes (PEC) used in this work are chitosan, obtained from the deacetylation of chitin from crusteans' shells, poly-L-lysine, widely used in biomedical field, and polyethylenimine. Chitosan oligosaccharide lactate (CHL) ($M_w \approx$ 5 kDa, pK_a ~6.5)[56] with a deacetylation degree >90%, poly-L-lysine (PLL) hydrobromide ($M_w \approx$1-5 kDa, pK_a ~10-10.5)[57] and polyethylenimine (PEI) hydrochloride (linear, $M_w \approx$ 4 kDa, pK_a ~8)[58] are purchased from

Sigma-Aldrich. All other chemicals are of reagent grade and are used without further purification.

Preparation of stock solutions

SL-C18:0 (C= 5 mg·mL^{-1}), G-C18:1 (C= 5 mg.mL^{-1}, C= 20 mg·mL^{-1}), CHL (C= 2 mg·mL^{-1}), PLL (C= 5 mg·mL^{-1}, C= 20 mg·mL^{-1}), and PEI (C= 5 mg·mL^{-1}) stock solutions (V= 10 mL) are prepared by dispersing the appropriate amount of each compound in the corresponding amount of Milli-Q-grade water. The solutions are stirred at room temperature (T= 23 ± 2 °C) and the final pH is increased to 11 by adding a few µL of NaOH (C= 0.5 M or C= 1 M).

Preparation of samples

Samples are prepared at room temperature (T= 23 ± 2°C) by mixing appropriate volume ratios of the lipid (SL-C18:0 or G-C18:1) stock solutions at pH 11 and cationic polyelectrolyte stock solutions (PEC), as defined in Table 1. The final total volume is generally set to V= 1 mL or V= 2 mL, the solution pH is about 11 and the final concentrations are given in Table 1. The pH of the mixed lipid-PEC solution is eventually is decreased by the addition of 1-10 µL of a HCl solution at C= 0.5 M or C= 1 M. pH has been changed by hand and by mean of a push-syringe device. The rate at which pH is changed is generally not controlled although it is in the order of several µL·min^{-1}. Differently than in other systems,[34,59] we did not observe unexpected effects on the PESC structure to justify a tight control over the pH change rate.

Table 1 – Relative volumes of lipid and cationic polyelectrolyte (PEC) solutions to mix to obtain given concentrations

Volume			Concentration	
Lipid stock solution / mL	PEC stock solution / mL	Water / mL	C_{Lipid} / mg·mL^{-1}	C_{PEC} / mg·mL^{-1}
0.5	0.5	0	2.5 or 10	2.5 or 10
	0.25	0.25	2.5	1.25
	0.125	0.375	2.5	0.625

Turbidimetric titration using UV-Vis spectroscopy

The influence of pH and concentration of PEC on the formation of coacervate droplets is investigated by measuring the absorbance at a wavelength of λ= 450 nm. Data are recorded at room temperature (T= 23 ± 2 °C) using a UV/Vis spectrophotometer (UVIKON XL, BioTek). Preparation of the samples for these experiments is the same as described above, however, the final concentration of the lipid is systematically set at C= 2.5 mg.mL^{-1}, while the final concentrations of the PEC range between 0.25 < C / mg·mL^{-1} < 1 for CHL and 0.63 < C / mg·mL^{-1} < 2.5 for PLL and PEI. The titrated volume is systematically V= 1 mL. The pH of each lipid-PEC mixed solution is decreased progressively by the manual addition of small amounts (V <10 µL) of HCl= 0.1 M. The turbidity curves are recorded after each pH variation. Each solution is stirred before analysis, which is however performed at rest under static conditions, thus favoring sedimentation during the measurement. The turbidity curve of control lipid and PEC solutions is also measured as a function of pH.

Turbidimetric titration using Light Scattering (LS) and ζ-potential

To avoid sedimentation, we have repeated the turbidimetric titration experiment on selected samples using the automatic titration unit MPT-2 of a Malvern Zetasizer Nano ZS90 (Malvern Instruments Ltd, Worcestershire, UK) instrument, equipped with a 4 mW He-Ne laser at a wavelength of λ= 633 nm, measuring angle, θ = 90°, temperature, T= 25°C, and the signal is never attenuated throughout the entire experiment. The sample solution (V= 7 mL) is contained in an external beaker and pumped with a peristaltic pump through the ζ-potential cuvette cell located in the instrument for analysis. pH is adjusted in the beaker by adding aliquots of V= 6 µL of a HCl solution at C= 0.5 M and controlled by the MPT-2 Zetasizer software. The beaker undergoes gentle stirring to avoid the formation of air bubbles in the flow-through tubing system and, consequently, in the ζ-potential cuvette. Avoiding air bubbles in the cuvette is crucial and accurately inspected throughout the experiment. Light scattering and ζ-potential are simultaneously recorded between each pH variation while the sample solution is continuously pumped through the cuvette. The latter action guarantees that sedimentation occurs neither in the cuvette nor in the external beaker.

pH-resolved in situ Small angle X-ray scattering (SAXS)

In situ SAXS experiments during pH variation are performed at room temperature on two different beamlines. The B21 beamline at Diamond Light Source Synchrotron (Harwell, England) is employed using an energy of E= 13.1 keV and a fixed sample-to-detector (Eiger X 4M) distance of 2.69 m. The Swing beamline at Soleil Synchrotron (Saint-Aubin, France) is

employed using an energy of E= 12 keV and a fixed sample-to-detector (Eiger X 4M) distance of 1.995 m. For all experiments: the q-range is calibrated to be contained between ~$5{\cdot}10^{-3}$ < $q/\text{Å}^{-1}$ < ~$4.5{\cdot}10^{-1}$; raw data collected on the 2D detector are integrated azimuthally using the in-house software provided at the beamline and so to obtain the typical scattered intensity *I(q)* profile, with q being the wavevector ($q = {4\pi \sin\theta}/{\lambda}$, where 2θ is the scattering angle and λ is the wavelength). Defective pixels and beam stop shadow are systematically masked before azimuthal integration. Absolute intensity units are determined by measuring the scattering signal of water ($I_{q=0}$= 0.0163 cm^{-1}). SAXS profiles are treated with SasView software, version 3.1.2, available at the developer's website (sasview.org).

The same sample experimental setup is employed on both beamlines: the sample solution (V= 1 mL) with the lipid and PEC at their final concentration and pH ~11 is contained in an external beaker under stirring at room temperature (T= 23 ± 2°C). The solution is continuously flushed through a 1 mm glass capillary using an external peristaltic pump. The pH of the solution in the beaker is changed using an interfaced push syringe, injecting microliter amounts of a 0.5 M HCl solution. pH is measured using a micro electrode (Mettler-Toledo) and the value of pH is monitored live and manually recorded from the control room via a network camera pointing at the pH-meter located next to the beaker in the experimental hutch. Considering the fast pH change kinetics, the error on the pH value is ± 0.2.

Cryogenic transmission electron microscopy (cryo-TEM)

Cryo-TEM experiments are carried out on an FEI Tecnai 120 twin microscope operated at 120 kV and equipped with a Gatan Orius CCD numeric camera. The sample holder is a Gatan Cryoholder (Gatan 626DH, Gatan). Digital Micrograph software is used for image acquisition. Cryofixation is done using a homemade cryofixation device. The solutions are deposited on a glow-discharged holet carbon coated TEM copper grid (Quantifoil R2/2, Germany). Excess solution is removed and the grid is immediately plunged into liquid ethane at -180°C before transferring them into liquid nitrogen. All grids are kept at liquid nitrogen temperature throughout all experimentation. Cryo-TEM images have been treated and analyzed using Fiji software, available free of charge at the developer's website.[60]

^{1}H solution Nuclear Magnetic Resonance (NMR)

^{1}H solution NMR experiments are performed on a Bruker Avance III 300 spectrometer using a 5 mm 1H-X BBFO probe. The number of transients is 32 with 7.3 s recycling delay, an

acquisition time of 2.73 s and a receiver gain of 322. We have employed a 5 mm NMR tube containing 500 µL of solution. The latter is obtained upon solubilization of a dried pellet in MeOD, also containing 3-(Trimethylsilyl) propionic-2,2,3,3-d_4 acid sodium salt (TMSP-d4) at 1 $mg.mL^{-1}$ (5.8 mM). The pellet is obtained by centrifugation of a solution at final pH of 5 containing the lipid and the polyelectrolyte and prepared according to the method described in the "Preparation of samples" paragraph in this section. After centrifugation, the supernatant is removed and the pellet is dried in an oven at 40°C for 2 days. These conditions have been kept constant throughout all experiments.

Isothermal Titration Calorimetry (ITC)

ITC experiments were performed using a TAM III isothermal calorimeter from TA Instruments. All the solutions (buffer pH 5.8, PLL 2 mM, G-C18:1 2 mM, and G-C18:1 4 mM) were degassed by 15 min sonication under vacuum. ITC experiments employ phosphate buffer solutions (NaH_2PO_4/Na_2HPO_4,10 mM) at pH 5.8. The titration experiments between PLL and G-C18:1 were performed with PLL 2 mM in the calorimetric cell and G-C18:1 (2 or 4 mM) solution in the syringe. Preliminary experiments (not shown) showed that high stirring rates (120 rpm) result in an unstable stable calorimetric trace most likely due to the foaming of the G-C18:1 despite the degassing step. This was also confirmed by visual inspection of the retracted measurement cell. For this reason, the experiments are conducted at a lower stirring speed of 30 rpm and with the G-C18:1 solution in the syringe. Prior to the start of the titrations, the system was equilibrated at 25°C until baseline variation was less than 50 nW/h. After calibration (dynamic and gain), 20 injections of 10µL each of G-C18:1 (2 or 4 mM) were successively added at 20 min intervals into the cell containing 0.8 mL of PLL 2 mM. A blank titration experiment to estimate the heat of dilution was also performed under the same conditions by injecting the buffer solution into PLL 2 mM. The calorimetric results were corrected for the heat of dilution by subtracting the blank experiment from the actual experiments. The data was fitted with a multi site model using NanoAnalyse data analysis software (TA Instruments) in order to determine the thermodynamic as well as the reaction parameters of the interaction between PLL and G-C18:1. From the enthalpy (ΔH) and the binding constant (K_a) of the reaction, the entropy (ΔS) and the Gibbs free energy (ΔG) of reaction were calculated using the following equation:

$$\Delta G = \Delta H - T\Delta S = -RTln(K_a)$$

Results

Deacetylated acidic sophorolipid SL-C18:0 (saturated) and glucolipid G-C18:1 (monounsaturated) are two microbial glycolipid biosurfactants used in this work and both containing a free carboxylic acid chemical function (Figure 1). Alkaline solutions of SL-C18:0 and G-C18:1 at room temperature and concentrations below 10 wt% are characterized by a major micellar phase. At pH< 7.4, SL-C18:0 self-assembles into crystalline twisted ribbons, while at pH< 6.2 G-C18:1 self-assembles into vesicles.[49,54,55]

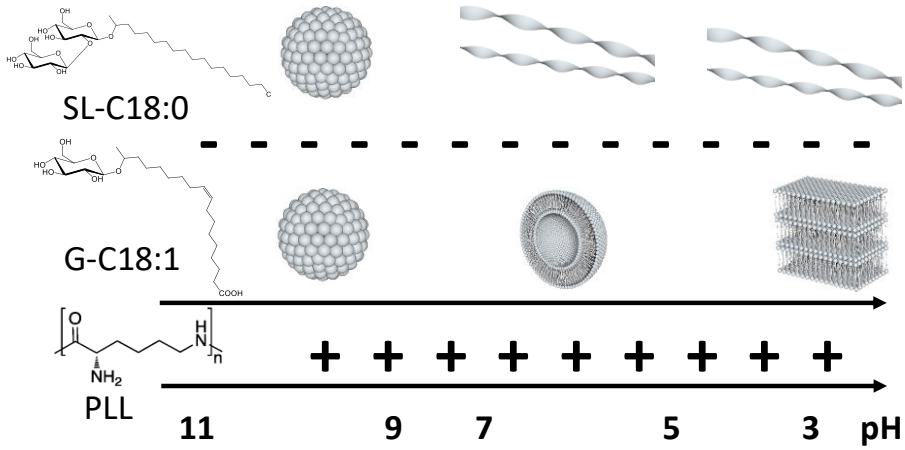

Figure 1 – pH-dependent phase and (negative) charge diagram for SL-C18:0 and G-C18:1 microbial glycolipids biosurfactants at C< 10 wt% and room temperature. The (positive) charge of PLL polyelectrolyte is also indicated as a function of pH

Figure 1 summarizes the pH-dependent phase and charge diagram of SL-C18:0 and G-C18:1 glycolipids, which are negatively charged above pH ~4.5, due to their carboxylate function. PLL polyelectrolyte is on the contrary positively charged below pH 10, water-soluble and it adopts a random coil conformation. The other PEC employed in this work, CHL and PEI, have a similar behavior, except for their pK_a values, which are respectively 6.5 and 8. The charge complementarity between the glycolipids and PEC in a given pH range leads to an expected electrostatic interaction, and which was shown to form glycolipid-PEC complex coacervates, when acidic deacetylated monounsaturated sophorolipids (SL-C18:1) were employed.[53] To explore whether SL-C18:0 and G-C18:1 glycolipids form complex coacervates, and whether their pH-induced phase transition has a potential impact on the coacervate structure, we perform a series of pH-stimulated experiments on mixtures of each glycolipid and PEC. The main body of this work summarizes the results obtained with PLL, while the data

collected on CHL and PEI are only briefly discussed and presented as supporting information, as they support the main conclusions obtained with PLL.

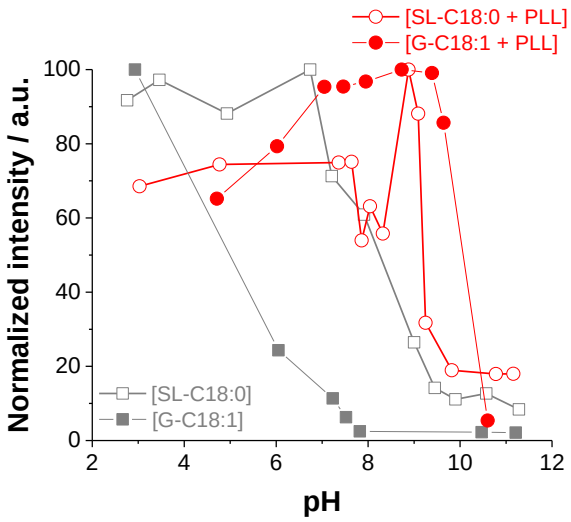

Figure 2 – Room temperature turbidimetric analysis performed by UV-Vis spectroscopy of SL-C18:0 and G-C18:1 glycolipid solutions with and without PLL as a function of pH. The typical sample preparation is described in the materials and method section. The final lipid and PEC concentrations are $C_{G\text{-}C18:1}$= $C_{SL\text{-}C18:0}$= 2.5 mg·mL^{-1}, C_{PLL}= 1.25 mg·mL^{-1}. pH is decreased from 11 to 3.

Figure 2 presents the pH-resolved turbidimetric analysis on control lipid ([SL-C18:0] and [G-C18:1]) solutions (grey symbols) and mixtures of lipids with PLL (red symbols). As a general result, control solutions display poor scattering (micellar phase) above pH ~8 and ~9 for, respectively, G-C18:1 and SL-C18:0; on the contrary, scattering is maximized below pH ~6 and ~7 for, respectively, G-C18:1 and SL-C18:0. These results are in agreement with their respective micelle-to-vesicle[49] and micelle-to-fiber[55] phase transitions. One must notice that scattering of SL-C18:0 fibers below pH 7 is weaker than what it should be[55] and this is due to sedimentation issues during the experiment. A specific comment on this aspect is associated to Figure S 1 in the Supporting Information and where pH-resolved experiments are performed *in situ* in the light scattering apparatus. Finally, scattering of PLL alone is negligible on the entire pH range and for this reason it is not displayed in Figure 2. Mixtures of SL-C18:0, or G-C18:1, and PLL highlight a region of strong scattering (red symbols) already at 9 < pH < 10, that is at least two to three orders of pH higher than the controls, and indicating that both glycolipids preferentially interact with PLL under these pH conditions, according to the likely hypothesis of charge matching schematized in Figure 1. The data in Figure 2, reported for final concentrations of lipid and PLL of, respectively, 2.5 mg·mL^{-1} and 1.25 mg·mL^{-1}, are quite robust and reproducible for a broader range of lipid-to-PLL mass ratios, as shown in Figure S 2.

Similar results were also reported for SL-C18:1 sophorolipids and PEC soutions[53] and for a broad range of micelle-polyelectrolyte complex coacervates.[21] pH-resolved *in situ* ζ-potential measurements are employed to show mutual interactions by charge-matching (Figure S 3). The lipid control solutions display the presence of negatively-charged colloids between pH 10 and 4, while lipid and PLL mixed solutions show an overall charge neutralization process occurring since pH 10, indirectly demonstrating the interaction between the lipid and polyelectrolyte, supported by both NMR and ITC presented later in the manuscript.

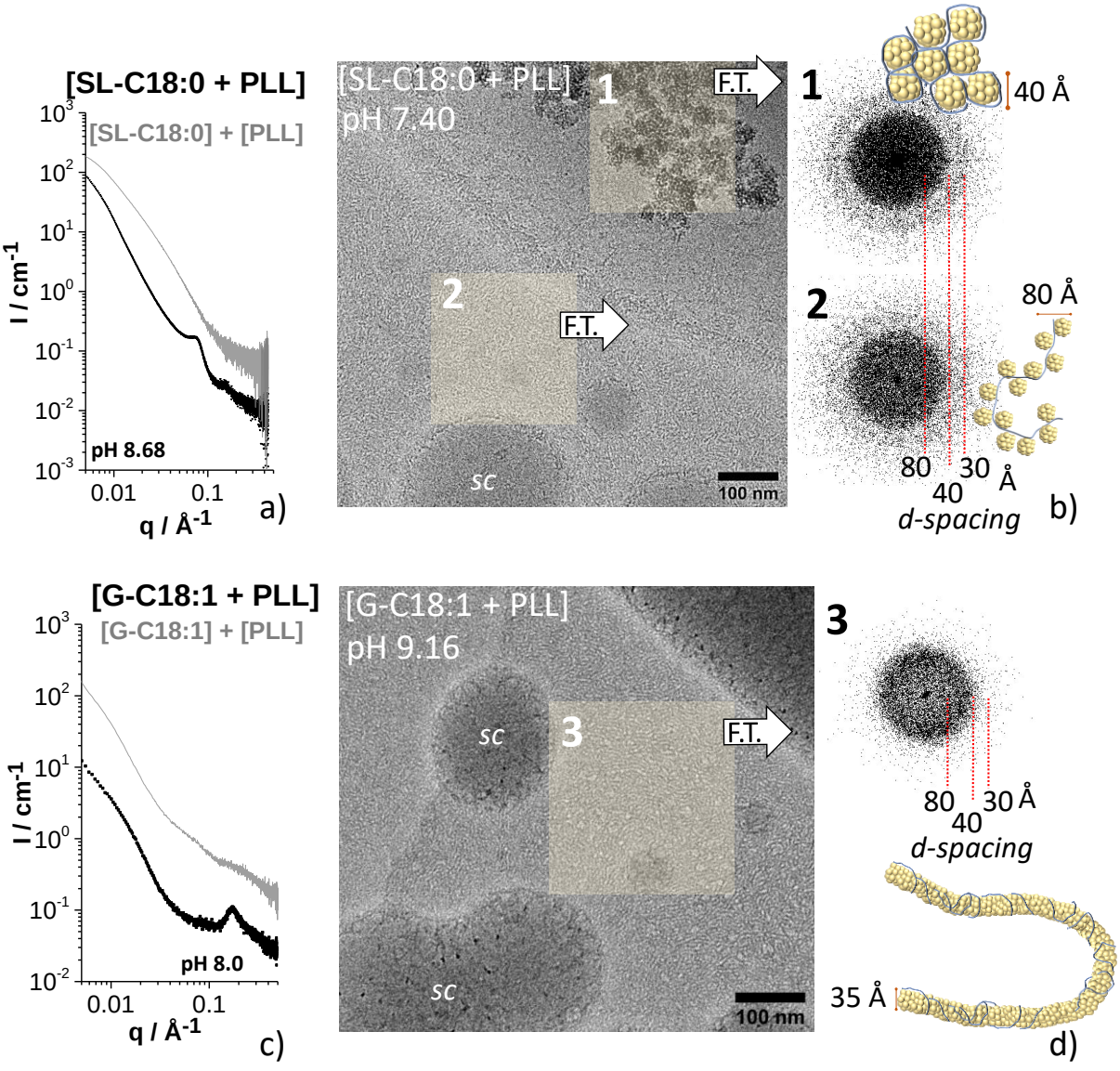

Figure 3 – a) SAXS profile recorded for a co-assembled mixture of [SL-C18:0 + PLL] (black curve) at pH 8.68. Grey curve: arithmetical summation of the SAXS profiles each recorded individually on the control solutions of [SL-C18:0] and [PLL] at pH 8.68. An artificial offset has been added for sake of clarity. Concentrations: $C_{SL\text{-}C18:0}$= C_{PLL}= 2.5 mg·mL^{-1}. b) Cryo-TEM image of the co-assembled [SL-C18:0 + PLL] solution at pH 7.40. Concentrations: $C_{SL\text{-}C18:0}$= 2.5 mg·mL^{-1}, C_{PLL}= 1.25 mg·mL^{-1}. Panels 1 and 2 identify regions where Fourier Transform (F.T.) is performed. F.T. images are indicated by the arrows on the right-

hand side of each cryo-TEM image. c) SAXS profile recorded for a co-assembled mixture of [G-C18:1 + PLL] (black curve) at pH 8.0. Grey curve: arithmetical summation of the SAXS profiles each recorded individually on the control solutions of [G-C18:1] and [PLL] at pH 8.0. An artificial offset has been added for sake of clarity. Concentrations: $C_{G\text{-}C18:1}$= C_{PLL}= 10 mg·mL^{-1}. d) Cryo-TEM image of the co-assembled [G-C18:1 + PLL] solution at pH 9.16. Concentrations: $C_{G\text{-}C18:1}$= 2.5 mg·mL^{-1} and C_{PLL}= 1.25 mg·mL^{-1}. The F.T. of panel 3 is shown on the right-hand side. Images have been analyzed using Fiji software.[60]

A combination of SAXS and cryo-TEM experiments (Figure 3 and Figure 4) is used to study the structure of SL-C18:0 and G-C18:1 with PLL in the regions of strong light scattering and below pH 7 (Figure 2). The SAXS profiles show the signals recorded at basic (Figure 3a,c) and acidic (Figure 4a,c) pH, where black curves labelled [SL-C18:0 + PLL] and [G-C18:1 + PLL] correspond to co-assembled lipid:PLL PESCs solutions. Grey curves labelled [SL-C18:0] + [PLL] and [G-C18:1] + [PLL] correspond to the arithmetic sum of the SAXS profiles recorded on the individual lipid and PLL controls solutions separately. Figure S 4 illustrates the SAXS profiles of the individual SL-C18:0 (blue symbols) and PLL (red symbols) control solutions recorded at pH 5.50 and 8.68 as well as their arithmetic sum (grey symbols). The difference in concentration between the G-C18:1 system at pH 8.0 (C= 10 mg·mL^{-1}) and the rest (C= 2.5 mg·mL^{-1}) is simply a matter of signal-to-noise ratio. The corresponding SAXS profile collected at $C_{G\text{-}C18:1}$= C_{PLL}= 2.5 mg·mL^{-1} and pH 8.0 is given in Figure S 5 and it indeed shows a similar profile but with a poorer signal-to-noise, probably due to a combination of poor contrast and low concentration.

Study of the complex coacervate (Co) phase

In the micellar region of the phase diagram (pH> 8), both glycolipids in their mixture with PLL have SAXS profiles characterized by a strong low-q scattering and a broad peak (black curves in Figure 3a,c). The peak is centered at q= 0.078 Å^{-1} (d= 80.5 Å) while a second peak can be observed at q= 0.15 Å^{-1} (d= 41.8 Å) for SL-C18:0 and at q= 0.174 Å^{-1} (d= 36.1 Å) for G-C18:1. Comparison between the co-assembled lipid and PLL solution (black curves) with the corresponding controls (grey curves in Figure 3a,c above pH 8) at basic pH shows that, if low-q scattering is generally comparable, the correlation peak is unique only in the co-assembled solutions and never observed for the pure glycolipids. The presence of a correlation peak is actually general and not only observed with PLL. For instance, SL-C18:0 (at basic pH) systematically shows two broad correlation peaks centered at q= 0.078 ± 0.002 Å^{-1} and at q= 0.15 ± 0.10 Å^{-1} when it is co-assembled with PLL, PEI or CHL (Figure S 6a). These peaks, common in scattering experiments of micelle-polyelectrolyte complex coacervates,[21] are

generally associated to the structure of the co-assembled lipid with PEC. To better understand the origin of the peak at basic pH in the SAXS experiments, we study the structure of [SL-C18:0 + PLL] and [G-C18:1 + PLL] using cryo-TEM.

The typical cryo-TEM images of [SL-C18:0 + PLL] and [G-C18:1 + PLL] at basic pH are shown in Figure 3, while additional images are given in Figure S 7. All samples, irrespective of the pH value, are characterized of large spherical colloidal (*sc*) structures, of diameter larger than 1000 Å, embedded in a medium, which often displays a fingerprint-like texture (panels 2 and 3 in Figure 3, Figure S 7a,d,e). Regions of much smoother, untextured, background are however observed, as well (Figure S 7b,c). *sc* display as dense, untextured, more contrasted, objects. One can occasionally observe, mainly in [SL-C18:0 + PLL] systems, a third type of component, constituted of agglomerated, highly contrasted, particles of typical primary size contained between 20 nm and 50 nm (panel 1 in Figure 3, Figure S 7b). Both aggregated particles and *sc* of similar texture, size, morphology and contrast were largely documented using cryo-TEM by us[53] and by others[23,61,62] in polyelectrolyte-surfactant complex coacervates.

The entire set of cryo-TEM images that we have recorded on glycolipids SL-C18:0 and G-C18:1 co-assembled with PLL or PEI at basic pH show the same type of structures as presented in Figure 3 and Figure S 7. From a macroscopic point of view, all samples form a stable suspension of liquid spherical droplets similarly to our previous results,[53] rather than a solid precipitate. The combination of these pieces of evidence[3] indicate that complex coacervation systematically occurs in the micellar region of the glycolipids phase diagram. Concerning CHL, we cannot draw a clear-cut conclusion due to the fact that this compound precipitates above pH 7[63] and its interactions with glycolipids in the alkaline region are at the moment unclear. The SAXS data corresponding to [SL-C18:0 + CHL] shown in Figure S 6 confirm this assumption: the typical correlation peaks, clearly observed in the PLL and PEI systems, can be hardly identified. However, complementary data recorded on the [G-C18:1 + CHL] system, and presented elsewhere,[64] still suggest the formation of complex coacervates.

Agglomerated, highly contrasted, particles (e.g., panel 1 in Figure 3) are generally attributed to dehydrated complex coacervates driven by microscopic electroneutrality[23,53] on the coacervation plateau, while *sc* structures surrounded by a textured backround (e. g., panel 2 and 3 in Figure 3) are attributed to sections of 3D hydrated complex coacervates structures at the point of macroscopic coacervation.[62] Dense structures are always superimposed to a clear background, as described by Dubin *et al.*,[23] while the fingerprint-like background is systematically associated to *sc* structures, independently of the glycolipid employed. This is nicely shown for [SL-C18:0 + PLL] in Figure 3b, where a clear-cut frontier delimitates dense

coacervates on top from *sc* on the bottom, the former being embedded in a smooth background while the latter embedded in a fingerprint-like background. In line with Dubin *et al.*,[62] we speculate that the composition of the fingerprint-like background is rich in glycolipid, while *sc* are rather rich in PEC. Probably due to the kinetic control of coacervation process, we are unable to establish the physicochemical conditions that could favor either dense aggregates or *sc* regions, as we observe both of them irrespectively of the pH value (Figure S 7a-c), or even coexisting at the same pH (Figure 3b). Nonetheless, we propose a structural interpretation through a crossed SAXS-cryo-TEM analysis of both [SL-C18:0 + PLL] and [G-C18:1 + PLL] systems.

The Fourier Transform (F.T.) of the fingerprint-like region in the [SL-C18:0 + PLL] system (panel 2 in Figure 3b) provides a broad ring corresponding to *d*-spacing between 80 Å and 40 Å, while the dense coacervate region, panel 1 in Figure 3b, provides an additional ring of *d*-spacing between 30 Å and 40 Å. Comparison between the *d*-spacing values estimated from cryo-TEM with *d*-spacing obtained by SAXS (*d*= 80.5 Å and *d*= 41.8 Å, Figure 3a) confirms the hypothesis according to which the correlation peak in SAXS is reasonably associated to the structure of complex coacervates. Interestingly, the *q*-values are in a 1:2 ratio, generally found in lamellar stacking but excluded in this system by cryo-TEM arguments. Correlation peaks with *q*-values in 1:2 ratio were observed before in β-lactoglobulin(βLgA)-pectin complex coacervates[65] and were attributed to the presence of βLgA clusters coexisting with ordered protein-to-protein correlations observed inside the clusters. In the present case, the *d*-spacing at *d*= 41.8 Å can be reasonably attributed to the dense aggregates (panel 1 in Figure 3b), most likely composed of tightly packed SL-C18:0 micelles embedded in the polyelectrolyte matrix adopting a globular conformation (Figure 3b).[23] This hypothesis is also in agreement with the typical cross-sectional diameter of SL-C18:0 micelles (~35 Å)[49] and with the previously-proposed colloid cluster model in complex coacervates.[21] However, the colloid cluster model unfortunately explains neither larger *d*-spacing values nor the fingerprint-like textured background. The only way to explain a *d*-spacing value corresponding to approximately twice the size of a SL-C18:0 molecule is by considering a "pearl-necklace"-like structure, proposed long time ago for polyelectrolyte-micelles complexes,[4,7,35,66] and adapted to the present (Figure 3b) to account for the larger experimental *d*-spacing.

The Fourier Transform (F.T.) of the fingerprint-like region, panel 3 in Figure 3d, in the [G-C18:1 + PLL] system, also shows a broad ring with *d*-spacing values contained between 40 Å and 60 Å, a range which is overestimated by at least a factor 1.5 with respect to the *d*-spacing value measured by SAXS (*d*= 36.1 Å). Despite such a discrepancy, the lack of other organized

structures in cryo-TEM and the lack of other correlation peaks in SAXS suggest that the correlation peak should be attributed to the textured background identified in panel 3 in Figure 3d. However, a spontaneous question arises: why is the *d*-spacing value associated to the textured region in the [G-C18:1 + PLL] system correlated to the size of a single G-C18:1 molecule[49,54] and not to twice its size, as found for [SL-C18:0 + PLL]? The only reasonable answer that we can propose is the possibly different packing of G-C18:1 around the polyelectrolyte: instead of the expected micellar packing, G-C18:1 could form interdigitated wormlike micelles stabilized by the polyelectrolyte (scheme in Figure 3d), as also discussed for other polyelectrolyte-micelle complexes.[3,4,20,67] This hypothesis is not outrageous because wormlike micelles are experimentally found as a transitory phase during the micelle-to-vesicle transition in the PEC-free G-C18:1 aqueous system.[49] Analysis of the slope in, or even modelling of, SAXS profiles could certainly help to corroborate the hypotheses of "pearl-necklace" (Figure 3b) and wormlike (Figure 3d) models, as proposed by other authors.[35,68] However, any tentative analysis of our SAXS data in the log-log scale provide a dependence of the intensity on *q* around -3, which is typically found for fractal structures but which, unfortunately, does not bring any additional structural information on the present system. Cryo-TEM experiments show a multiphasic medium with coexistence of more than one structural intermediate, thus making a clear-cut interpretation of the SAXS profile very hard, if not impossible.

In the rest of the manuscript, the term *Co* phase will broadly refer to the complex medium in the basic pH region composed of aggregated structures (panel 1 in Figure 3), PEC-rich *sc* (Figure 3) and glycolipid-rich textured (panel 2,3 in Figure 3) regions.

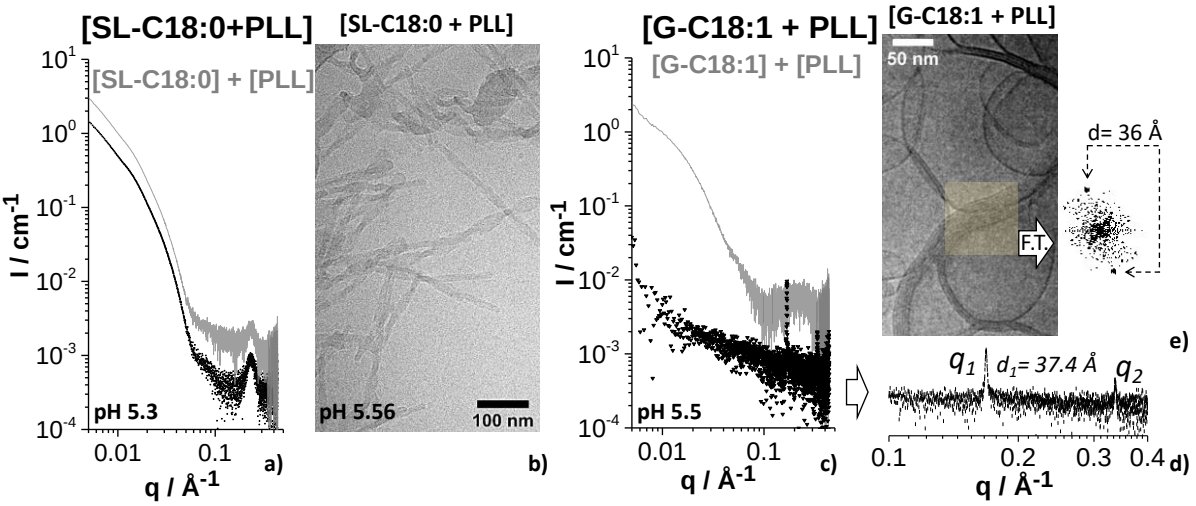

Figure 4 – a) SAXS profile recorded for a co-assembled mixture of [SL-C18:0 + PLL] at pH 5.30. Grey curve: arithmetical summation of the SAXS profiles each recorded individually on the control solutions of [SL-C18:0] and [PLL] at pH 5.30. An artificial offset has been added for sake of clarity. b) Cryo-TEM image of the co-assembled [SL-C18:0 + PLL] solution at pH 5.56. Concentrations in a-b) are $C_{SL\text{-}C18:0} = C_{PLL} = 2.5$ mg·mL^{-1}. c) SAXS profile recorded for a co-assembled mixture of [G-C18:1 + PLL] (black curves) at pH 5.50. Grey curve: arithmetical summation of the SAXS profiles each recorded individually on the control solutions of [G-C18:1] and [PLL] at pH 5.50. An artificial offset has been added for sake of clarity. d) Highlighted high-q region of [G-C18:1 + PLL] at pH= 5.50. e) Cryo-TEM image of the co-assembled [G-C18:1 + PLL] solution at pH 4.70. Concentrations in c-e) are $C_{G\text{-}C18:1} = C_{PLL} = 2.5$ mg·mL^{-1}. Images has been analyzed using Fiji software.[60]

In situ study of the lipid-PLL system below neutral pH

pH-resolved *in situ* SAXS is employed to study the lipid-PLL phase behavior below neutral pH. Experiments performed at acidic pH are shown in Figure 4a,b (SAXS: black curve, pH 5.30; cryo-TEM: pH 5.56) for the [SL-C18:0 + PLL] mixture and in Figure 4c-e (SAXS: black curve, pH 5.50; cryo-TEM: pH 4.70) for the [G-C18:1 + PLL] mixture. In the SL-C18:0 system, SAXS shows a strong low-q scattering and a diffraction peak at $q = 0.24$ Å^{-1}. The same exact profile is observed for the [SL-C18:0] + [PLL] control signal (grey curve, pH 5.30, Figure 4a) and reported for a typical aqueous solution of SL-C18:0 twisted ribbons, the peak being attributed to the repeating inter-lipid layer distance within each ribbon.[55] Twisted ribbons of similar size (cross section ~150 Å) and morphology compared to the previous findings of pure SL-C18:0 system at acidic pH are actually observed in the corresponding cryo-TEM images (Figure 4b). Knowing that SL-C18:0 assembles into a fibrillar phase at acidic pH, one can reasonably suppose that SL-C18:0 does not interact with PLL under these conditions and the micelle-to-fiber self-assembly process (Figure 1) occurs independently whether SL-C18:0 is in a free micellar[49,55] or in PESCs complex coacervates. At the moment, we do not have evidence, both by SAXS and cryo-TEM, later on confirmed by NMR arguments, that SL-C18:0 fibers interact in any way with PEC, differently than what was reported for the fibrillation of bile salts complexed with block copolymers.[46] We could explain this evidence by the fact that self-assembled fibers are only composed of the COOH form of SL-C18:0 and they are thus neutral objects, which do not interact with PEC. This statement seems to be in contrast with ζ-potential experiments performed on the SL-C18:0 system below pH 7 (Figure S 3) and showing an overall negative charge. However, one should be aware that ζ-potential experiments are not structure-selective and we have no direct proof that the global negative charge is specifically associated to fibrillar structures rather than to a set of coexisting colloids composed of fibers

and residual micelles. If fibers are actually negatively charged, one should also not exclude the possibility that the charge density is too low to drive complexation with PEC.

The SAXS profile of the [G-C18:1 + PLL] at pH 5.50 (black curve, Figure 4c,d) is on the contrary very different than the corresponding [G-C18:1] + [PLL] control signal (grey curve, pH 5.50, Figure 4c): the mixture displays two sharp peaks at q_1= 0.17 Å^{-1} and q_2= 0.34 Å^{-1} (Figure 4d), referring to the (100) and (200) reflection of a lamellar order, while the control signal has the typical profile of single-wall vesicles, expected for G-C18:1 in water at concentration below 10 wt% and pH< 7.[49,54] The q_1:q_2= 0.5 and the sharpness of the peaks (Δq= 1.4·10^{-3} Å^{-1}) strongly suggest the presence of extended lamellar domains, never observed for this compound alone prepared under the same conditions. The corresponding cryo-TEM image in Figure 4e interestingly shows the systematic massive presence of vesicular objects having a thick lamellar wall (white arrows in Figure 4e), as similarly found in lipoplex systems,[2,19] and other multilamellar walls vesicle PESCs,[4] where the lipid walls (here G-C18:1) are held together by the sandwiched polyelectrolyte (here PLL). Cryo-TEM excludes the presence of a flat lamellar phase, or condensed platelets. A more detailed electron microscopy study of the [G-C18:1 + PLL] material under acidic pH conditions are reported elsewhere.[64]

To better understand the phase transition from alkaline to acidic pH, Figure 5 shows the full range of the pH-resolved *in situ* SAXS experiment, presented as 2D contour plots.

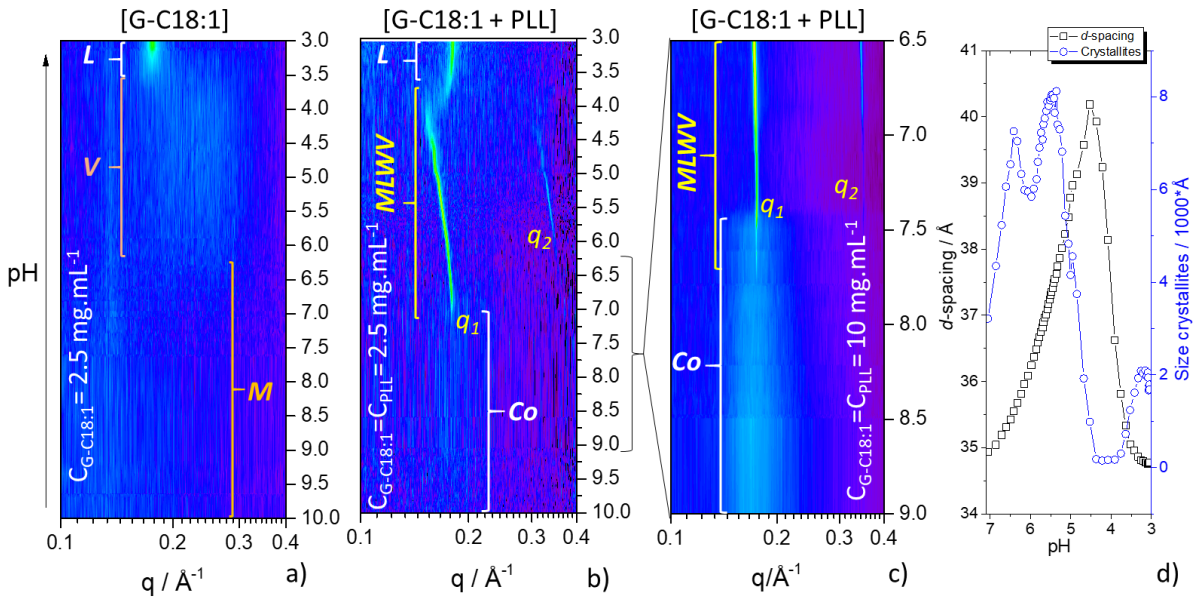

Figure 5 – pH-resolved (pH is changed from alkaline to acidic) *in situ* SAXS 2D contour plots of a) G-C18:1 control solution (C= 2.5 mg·mL^{-1}), b) [G-C18:1 + PLL] sample at $C_{G\text{-}C18:1}$= C_{PLL}= 2.5 mg·mL^{-1} and c) [G-C18:1 + PLL] sample at $C_{G\text{-}C18:1}$= C_{PLL}= 10 mg·mL^{-1}. *M*: Micellar phase; *V*: Vesicles phase; *L*: Lamellar phase; *MLWV*: Multilamellar wall vesicle phase; *Co*: Complex coacervate phase. d) Evolution of *d*-spacing

and size of crystallites at pH< 7 for experiment in b). *d*-spacing is obtained from 6.28/q_1 while size of crystallites is obtained using the Scherrer formula (0.9*6.28)/*FWMH*, where *FWHM* is the full width at half maximum of peak q_1 given in Å^{-1} units. q_1 and *FWHM* have been obtained by mean of a Lorentzian peak fitting procedure.

The contour plot (0.1 < q / Å^{-1} < 0.4) concerning the pH dependency of G-C18:1 control sample solution is shown in Figure 5a. The pH region between pH 10 and ~6.5 is characterized by no distinct signal in the contour plot representation, as expected, because G-C18:1 forms a micellar, *M*, phase in this pH range.[49,54] Below pH ~6.5 and until pH ~3.5, the contour plot shows a broad signal, characterizing the vesicle, *V*, phase and corresponding to the oscillation of the vesicle membrane form factor (grey profile, pH 5.5, Figure 4c) and largely documented in Ref. [49,54]. Below pH ~3.5, two sharp diffraction peaks at q= 0.176 Å^{-1} and q= 0.352 Å^{-1} (Figure S 8) refer to the (100) and (200) reflections of a lamellar order and characterize a lamellar phase, *L*, precipitate in solution.[49] In summary, the control G-C18:1 solution displays a micelle-to-vesicle-to-lamellar phase transition in agreement with our previous results.[49]

The contour plot for the [G-C18:1 + PLL] PESC at C= 2.5 mg·mL^{-1} is shown in Figure 5b. From pH 10 to about pH 7.5, the plot shows the dim signal of the broad (Δq= 0.06 Å^{-1}) correlation peak at q= 0.171 Å^{-1} attributed to the *Co* phase, of which the composition is defined earlier in the manuscript. Figure S 5 better highlights the peak, which is hardly observable in the contour plot due to a simple matter of plotting levels. The signal of the same phase is more intense and better identified at higher lipid and PLL concentration, as highlighted by the *Co* phase region between pH 9 and 7.5 in Figure 5c and Figure S 5. Below pH ~7.5, two sharp diffraction peaks of full width at half maximum Δq= 0.0015 Å^{-1}, respectively corresponding to the first and second order reflections, q_1 and q_2, of the multilamellar walls vesicle, *MLWV*, phase in Figure 4d,e, are observed until pH 4. Figure 5b shows that the position of q_1 (and q_2) varies continuously from q_1= 0.178 Å^{-1} at pH 7.5 to q_1= 0.157 Å^{-1} at pH 4, corresponding to a variation in *d*-spacing of 5 Å, between 35 Å to 40 Å (black squares in Figure 5d). Below pH 4, the contour plot is characterized by an abrupt jump in the q-value from 0.157 Å^{-1} back to 0.176 Å^{-1}, immediately stabilizing itself at 0.181 Å^{-1}, and corresponding to a similar decrease in *d*-spacing of 5 Å, from 40 Å back to 35 Å.

The q_1 peak below pH 4 has the same features (position, invariance of the position towards pH, appearance in the same pH range) as the peak characterizing the *L* phase of the control G-C18:1 solution (Figure 5a). We then reasonably attribute it to the precipitation of the lipid *L* phase, probably without PLL, which is most likely expelled in the surrounding solution.

This assumption will be discussed in more detail in the next paragraphs. All in all, the G-C18:1 lipid undergoes a pH-driven *Co*-to-*MLWV*-to-*L* phase transition when mixed with PLL. In fact, this result is more general and not restricted to PLL only: we find similar results for all other PEC tested in this study and discussed elsewhere.[64]

In comparison to G-C18:1, SL-C18:0-based PESCs behave in a completely different manner, because they are characterized by a straight micelle-to-fiber phase transition around pH 7. No structural or morphological continuity in the micelle-to-fiber phase transition is ever observed for this system, where micelles are more thought to play a reservoir role rather than a nucleation site.[49,59] Interestingly, when SL-C18:0 is mixed with PLL, we also observe a systematic direct coacervate-to-fiber phase transition (Figure S 9), where the coacervate signal signal (q= 0.078 Å^{-1}; q= 0.15 Å^{-1}) at basic pH fades away until the appearance of the typical fiber structural peak at q= 0.229 Å^{-1} below pH 7.[49] This behavior follows the direct micelle-to-fiber phase transition observed for the SL-C18:0 control and we could reproduce it with all PEC employed in this work when they are mixed with this lipid.

Complex coacervate-to-Multilamellar wall vesicles (Co-to-MLWV) phase transition

The pH-resolved *in situ* SAXS experiments show a remarkably different behaviour of the G-C18:1 lipid in the presence of PLL with respect to the control. The latter undergoes a micelle-to-vesicle phase transition, driven by the carboxylate-to-carboxylic acid reaction upon lowering the pH and inducing a conformational change of the lipid. Low curvature membrane (Figure 6b) morphologies are then favoured over high curvature micelles (Figure 6a), due to the progressive disappearance of repulsive electrostatic interactions, which indirectly impact the packing parameter of the lipid.[18,69] Our data show that the same phenomenon occurs in the presence of PLL, when the lipid micelles are engaged in the formation of complex coacervates (Figure 6c). Upon lowering the pH, micelle-to-vesicle phase transition always occurs despite the presence of PLL; however, instead of forming single-wall vesicles, classically found in the control,[54] we observe a *Co*-to-*MLWV* phase transition (Figure 6d).

The continuity in the phase transition and the isostructural and isodimensional correlations between the coacervate and *MLWV* phases is explicit in the 2D SAXS experiment at $C_{\text{G-C18:1}}$= 10 mg·mL^{-1} (Figure 5c): the broad correlation peak of the *Co* phase at q= 0.171 Å^{-1} fades away between pH 7.7 and 7.5 and it overlaps to the sharp diffraction peak of the *MLWV* phase at q_1= 0.179 Å^{-1}. Their position only shifts in $|q-q_1|$ = 0.007 Å^{-1} (1.6 Å) strongly suggesting an internal, progressive, restructuring of the coacervates into *MLWV* (Figure 6c,d). The average d-spacing associated to the q range contained between 0.171 Å^{-1} and 0.179 Å^{-1} is

d= 35.9 Å, in agreement with both the typical diameter of a G-C18:1 micelle and the thickness of its corresponding membrane,[49] but also to the length of a single lipid molecule, estimated to be about 25 Å using the Tanford relationship.[54,70] G-C18:1 is a bolaform amphiphile and we have previously shown that its micellar structure is not a classical core-shell spheroid, where the diameter roughly corresponds to twice the size of the molecule,[71] but rather to a core-shell ellipsoid, where the diameter matches the size of each single lipid, a typical behavior in bolaamphiphiles (Figure 6a,c).[49,71,72] In the meanwhile, we have also shown that, differently than bilayer-forming lipids, G-C18:1 forms vesicles with an interdigitated lipid layer (IL), of which the thickness corresponds to the size of a single molecule (Figure 6b,d).[49,54,71,72] In light of these observations, the most reasonable hypothesis explaining the *Co*-to-*MLWV* transition is a local decrease in curvature due to the micelle-to-IL transition (Figure 6c,d) of G-C18:1. The driving force is the screening of electrostatic repulsions between adjacent carboxylate groups due to progressive acidification (Figure 6a,b). The residual negative charges in the membrane guarantee a charge density high enough to promote electrostatic attraction with the positively-charged PLL contained between two G-C18:1 IL, as theoretically predicted and experimentally observed in polyelectrolyte systems at charged interfaces.[41,73,74]

The equilibrium curvature in lipid-polyelectrolyte complexes depends on a subtle force balance between the bending modulus and electrostatic energy, which can be comparable.[38,39,75] Polymers can have a significant impact on the bending energy of lipid bilayers in the case of strong adsorption and large polymer volume fractions.[36] For charged systems in particular, the interplay between the bending stiffness of the lipid bilayer and the charge density of both the lipid bilayer and polyelectrolyte govern the overall free energy of the complex.[4,25,38,39,75] As a consequence, it is not obvious to predict the equilibrium curvature in a complex polyelectrolyte-bilayer system at equilibrium,[42,43] and this task becomes even harder, if not impossible, in non-equilibrium systems with variable surface charge density.

Micelles have a high charge density and a higher spontaneous curvature compared to vesicles. When the decrease in pH reduces the charge density inducing the micelle-to-vesicle phase transition, the PESC undergoes the *Co*-to-*MLWV* phase transition, meaning a decrease in spontaneous curvature. Interestingly, the pH region where this phenomenon occurs is the same in the control and in the complex, thus meaning that the contribution of the membrane bending energy prevails over the electrostatic energy contribution.[38] It is also interesting to note that [G-C18:1 + PLL] PESCs form vesicular (*MLWV*), and not flat, multilamellar objects. This is also not an obvious result and it can also be explained by the subtle interplay between the electrostatic and bending energies.[37,39] The former is not large enough to counterbalance the

membrane spontaneous tendency to bend; on the contrary, the magnitude of the latter, being proportional to the membrane bending rigidity,[76] is not high enough to drive the complex towards an infinitely small curvature, characterizing a flat structure.

In the description proposed by Brooks *et al*.[36], the effective bending energy can significantly vary in the case of strong adsorption and large volume fraction of the polymer, meaning that, in principle, the polymer could flatten the membrane. Other authors point at the importance of the charge ratio, *Z*, between the polyelectrolyte and the lipid but also at the persistence length, that is the rigidity, of the polymer:[7] for small *Z* and flexible polymers, supramicellar aggregates like complex coacervates are favoured, while for high *Z* and rigid polymers, micellar rods or flat bilayers might be favoured. In the present work we observe the same phase *Co*-to-*MLWV* transition, whichever the polymer employed, may it be PLL or chitosan, the latter being considered as rigid.[7] The ionic strength is not controlled but the pH change process generates salt concentrations generally below 50 mM, which are generally enough to keep the rigidity properties of the polyelectrolyte.[7] A specific comment on the ionic strength will be given at the end of the manuscript. The actual value of *Z* for our systems is harder to determine. A mere calculation based on the lipid and PEC concentrations and respective molecular weight indicates $Z< 1$, which is compatible, according to ref. [7], with the existence of complex coacervates. However, in these systems *Z* increases during pH variation because of the carboxylate-to-carboxylic reaction and in fact we are not able to quantify *Z* at a given pH simply because we cannot measure the actual surface charge density and distribution in PESCs. On the basis of these considerations, we conclude that the impact of polymer adsorption (including strength, quantity, rigidity and screening) is not strong enough to prevent the micelle-to-vesicle transition and to counterbalance the bending energy of the surfactant in the vesicle phase. For this reason, the stable phase is vesicular and not flat lamellar, as found at lower pH values.

In the *MLWV* phase, between pH 7.5 and 4, the *d*-spacing of the lamellar wall progressively increases from $d= 34.9$ Å ($q_1= 0.180$ Å^{-1}) to $d= 40.2$ Å ($q_1= 0.156$ Å^{-1}), before precipitation of the *L* phase below pH 4 with $d= 34.8$ Å ($q= 0.181$ Å^{-1}) measured at pH 3 (Figure 5d). At the moment of formation, *MLWV* have the same *d*-spacing value as in the *L* phase and this value is less than 1 Å shorter compared to the lamellar period in the G-C18:1 *L* phase control ($d= 35.7$ Å). The fact that the shortest *d*-spacing in the *MLWV* is comparable to the control is counterintuitive, because the interlamellar volume in the *MLWV* must accommodate PLL chains, which occupy a given volume. However, from the theory of polyelectrolyte adsorption on surfaces of opposite charges and from many experimental works, it is well-known

that polyelectrolytes can form a flat 2D layer.[74,77] In this case, the thickness of the polyelectrolyte layer corresponds to its molecular cross-section. The cross-sectional diameter of PLL is reasonably expected to be contained between 1 Å and 8 Å, the former being the lower limit found in many polymeric systems[78] and the latter estimated in bilayer/PLL multilayers at pH below 7.[79] The thickness of the G-C18:1 interdigitated layer can be calculated to be about 25 Å by applying the Tanford formula (L= 1.54+1.265*n, L being the length of the aliphatic chain and n the number of methylene groups)[70] to an effective C16 aliphatic chain (considering the 120° of the double bond in G-C18:1) and taking 8 Å as the size of a single glucose molecule.[80] Experimentally, we have estimated the thickness of the G-C18:1 membrane to be contained between 28 Å (pH 7) and 30 Å (pH 6) by modelling SAXS data (Figure S 4 in Ref. [49]), with an error due to fitting process of at least ±10 %. To account for the experimental *d*-spacing values, one has to consider a hydration interlamellar layer between 5.7 and 7.7 Å in the PLL-free control system, which can be classically found in lipid lamellar phases.[81,82] At the moment of formation of the *MLWV* at pH 7 (d= 34.9 Å), one can otherwise estimate the contribution of PLL to the interlamellar layer to be contained between 4.9 Å and 6.9 Å, the latter being in better agreement with what it was experimentally reported in ref. [79] and taking into account a thickness of the IL of 28 Å.

Several points should be highlighted from the above:

- Considering the thickness of the lipid membrane, the resulting interlamellar space is compatible with the diameter of PLL. In other words, a single PLL layer accommodates in between G-C18:1 interdigitated layers during the formation of *MLWV* in agreement with the dilute and semidilute regimes described in ref. [74].
- Considering the fact that the interlamellar distance is practically equivalent to the expected diameter of PLL, one does not expect a significant content of hydration water and counterions in the proximity of PLL. This is consistent with the entropic gain of releasing water molecule and counterions during the formation of PESCs,[4,25] verified and quantified below by ITC experiments. However, hydration water and counterions can fill the space between adjacent polyelectrolyte molecules, as also implied by the semidilute regimes described in ref. [74].
- At the moment of *MLWV* formation and after precipitation of the *L* phase below pH 4, the thickness of the interlamellar space is the same and it is comparable with the interlamellar thickness in the PLL-free control. This fact shows that PLL can partly replace hydration water, confirming the assumptions above.
- Considering that *d*-spacing is the same at the moment of *MLWV* formation at pH 7 and after precipitation of the *L* phase below pH 4, one could formulate the hypothesis that PLL is trapped

in the *L* phase. Our data cannot directly prove this assumption, but we will provide more insights on this point in the following paragraphs, suggesting that this is not the case.

- Increase of the *d*-spacing in the *MLWV* between pH 7 and pH 4 is certainly related to the protonation of G-C18:1, an analogous, although opposite, mechanism described for systems composed of lipid membrane with constant charge density and pH-reactive polyelectrolytes.[20] A more detailed explanation of the pH-dependent evolution profiles of both *d*-spacing and size of lamellar crystallites (Figure 5d) is given below.

- Reversibility of the *Co*-to-*MLWV* to *MLWV*-to-*Co* phase transitions is addressed on Figure S 10, of which a)-panel focuses on the alkaline-to-acidic *Co*-to-*MLWV* transition (C= 10 mg·mL^{-1}), discussed above, and b)-panel highlights the reversed acidic-to-alkaline pH variation performed on the same sample. Figure S 10b shows the lamellar peak of the *Co*-to-*MLWV* phase but it does not show any evidence of the correlation peak typical of the *Co* phase, indicating that the *Co*-to-*MLWV* phase transition is not reversible. This could be due to a number of reasons among which the screening effect of salt generated during the pH variation process, known to have a strong impact on the phase diagram.[25]

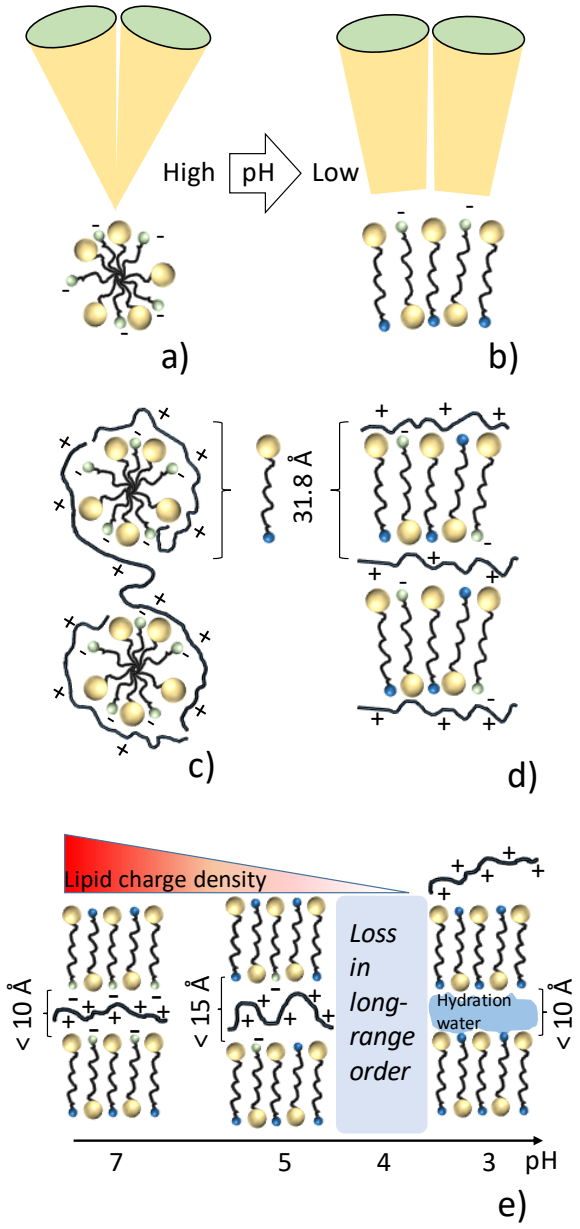

Figure 6 – Schematic view of the pH-driven transition between (a) micelles and (b) interdigitated membrane composed solely of G-C18:1. In the presence of PLL, the transition between the (a) complex coacervate and (b) the multi-lamellar wall in the *MLWV* occurs via a morphology change (micelle-to-vesicle) but a structural continuity (micelle-diameter ≈ membrane thickness). e) Insight on the evolution of the pH-dependent interlamellar spacing inside the multi-lamellar walls of *MLWV*: upon decrease in the membrane charge density, PLL expands and it applies a repulsive pressure to the lipid membranes. When the membrane is close to neutrality, long-range order is lost, *MLWV* disassemble, PLL is expelled and G-C18:1 precipitates into a hydrated lamellar phase.

The pH-dependent *d*-spacing evolution is explained by looking at the intermolecular forces equilibrating in the interlamellar space. In a polymer-free lipid bilayer system, attractive Van der Waals interaction counterbalances two short-range (< 30 Å), steric and hydration, and

two long-range (> 30 Å up to hundred of nanometers) repulsive interactions, electrostatic and thermal undulation.[83–85] For interlamellar spacing below 30 Å, which is the case here, electrostatic and undulation are generally neglected. In the case of a polyelectrolyte contained between membranes with variable charge density, which is the case in this work, one should consider additional terms in the energy balance like a repulsive free polymer term, including chain elasticity and excluded-volume terms, an entropic contribution of the small ions, an electrostatic contribution, containing the polyelectrolyte-surface attractive and inter-chain repulsive interaction.[40,41,73,74,86,87] Under the conditions of *MLWV* formation, around pH 7, the negatively-charged G-C18:1 membrane undergoes strong electrostatic attraction with PLL, largely-documented in both theoretical and experimental works on polyelectrolytes at charged interfaces.[41,73,74,87–89] When pH decreases, the carboxylate to carboxylic acid reaction reduces the number of negative charges and, consequently, it lowers the charge density of the lipid membrane. Since the attractive electrostatic component in the lipid-polyelectrolyte complex depends on the lipid charge density, lowering pH will reduce its contribution to the free energy. The consequence will be an increased volume occupied by the polyelectrolyte,[74] which will cause an increase in the repulsive osmotic pressure[40,41] with consequent swelling of the membranes, experimentally shown in Figure 5b,d and schematized in Figure 6e.

Below pH 4, the *MLWV* peak disappears until pH ~3, when the signal of the *L* phase at *d*= 34.8 Å appears again. Interestingly, this value is practically the same one observed at the moment of the *MLWV* formation at pH 7 and actually 0.9 Å smaller than the *d*-spacing found in the G-C18:1 control at the same pH value. Such an observation could induce to formulate the hypothesis that in the *MLWV*-to-*L* phase transition below pH 4, PLL is confined in between the lamellae. In fact, we believe that this is not the case for several reasons. It is well-known that at low hydration and in the absence of specific attraction interactions, large polymers segregate outside the lipid interlamellar space.[90] However, the polymer cannot be reasonably expelled from a dense, closed, multilamellar object. The evolution of the crystallite size with pH in Figure 5d helps understanding the mechanism of expulsion. Between pH 5 and 4, *d*-spacing is still increasing, testifying of the expansion of the lamellae due to the repulsive pressure applied by PLL. In the meanwhile, the peak becomes broader, with consequent drop in the crystallite size. At pH 4, the peak becomes so large that the crystallite size has dropped from several thousand of Ångstrom to only few Ångstrom, while *d*-spacing drops back to 34.7 Å. Below pH 5, the repulsive pressure exerted by PLL becomes so strong that the long-range order in the *MLWV* is lost. Complete disruption of the multilamellar walls occurs below pH 4, when PLL could eventually be expelled in the surrounding aqueous solution. Upon expulsion

of PLL, G-C18:1 precipitates in its thermodynamically favorable *L* phase, the same as found in the control lipid solution. This mechanism is summarized in Figure 6e at pH below 5.

Study of the interactions between glycolipids and PLL

To confirm and quantify the interactions between G-C18:1 and PLL in the *MLWV* phase, as hypothesized in Figure 6, and to prove that SL-C18:0 fibrils do not contain PLL, we run a combination of solution NMR and ITC experiments. ^{1}H NMR is employed to prove the presence (or absence) of PLL at pH 5, either in the fiber or *MLWV* phase. From ^{1}H NMR experiments, it is also possible to estimate the efficiency of the assembly process and the [COOH]-to-[NH_2] molar ratio. *MLWV* and fibers formed at pH 5 are centrifuged out of their parent solution, dried, dissolved in MeOD-d4 and analyzed by ^{1}H NMR employing an internal reference (0 ppm, TMSP-d4, C= 5.8 mM). The lipids are characterized by a well-defined triplet around 2.18 - 2.20 ppm ($RC\underline{H}_2C{=}O$) while PLL is characterized by a broad signal at 2.92 ppm [$(RC\underline{H}_2NH_2)_x$ ($x \sim 20$)].

In the [SL-C18:0 + PLL] system, only the peaks of SL-C18:0 are observed while the characteristic peak of PLL at δ = 2.92 ppm is not detected in any of the samples initially prepared at various SL-C18:0-to-PLL ratios (Figure S 11c,d). If SAXS and cryo-TEM data (Figure 4a,b) show the formation of twisted ribbons, NMR shows that their composition is only constituted by SL-C18:0, demonstrating, within the NMR sensitivity, that they do not contain PLL, thus confirming the absence of specific interactions between SL-C18:0 and PLL.

The characteristic peaks of both G-C18:1 (δ = 2.20 ppm) and PLL (δ = 2.92 ppm) are on the contrary observed in the *MLWV* phase (Figure S 11a,b), showing the simultaneous presence of both G-C18:1 and PLL, thus supporting the hypothesis of strong interactions between these compounds.

Table 2 shows the quantitative analysis of the NMR data (full integration data are given in Table S 1). The initial $\frac{[\mathrm{G-C18:1}]_{In}}{[\mathrm{PLL}]_{In}}$ molar ratio corresponds to the initial solution (exact concentrations are given in Table S 1), while $\frac{[\mathrm{G-C18:1}]_{F}}{[\mathrm{PLL}]_{F}}$ corresponds to the final ratio found in the *MLWV* phase. The former, also known as *r* in the literature,[21] is generally different than the latter, known as *r**.[21] This behaviour is expected and often reported for complex coacervate systems, which follow their own stoichiometry even if the initial ratio is not optimized.[21] $\frac{[\mathrm{G-C18:1}]_{F}}{[\mathrm{PLL}]_{F}}$ ranges between roughly 100 and 200, where the large discrepancy is in fact not so

surprising and probably due to the crude method to prepare the sample (centrifugation, redispersion) prior to NMR analysis.

From the above, one can estimate the final monomer ratio $\frac{[COOH]_F}{[NH_2]_F}$ in the *MLWV* phase and varying between 5 and 10. These numbers should be taken with caution for two reasons: 1) the large uncertainty on the M_w of PLL, here taken as 2.5 kDa but actually varying between 1 kDa and 5 kDa; 2) the uncertainty on the integral of PLL, which, being a high-molecular weight compound, may not be quantitatively probed by solution NMR due to long T2 relaxation times. Despite the uncertainty on the signal of PLL, $\frac{[COOH]_F}{[NH_2]_F}$ seems to show that interactions between G-C18:1 and PLL occur with an excess of carboxylic acids. In fact, simple considerations based on pKa and pH at which experiments are performed show that the actual charged monomer ratio, $\frac{[COO^-]_F}{[NH_3^+]_F}$, is in fact much closer to unity, as one would expect on the hypothesis of charge neutralization between G-C18:1 and PLL and in agreement with ζ–potential experiments (Figure S 3). *MLWV* are initially prepared at pH 5, where all amine are essentially protonated into NH_3^+ (pK_a ~10-10.5).[57] The pKa of the oleic acid moiety of G-C18:1 could be considered of about 7, a classical value found for oleic acid in water.[91,92] Then, the actual COO^- content at pH 5 could reasonably be estimated between 10% and 30%, for which $\frac{[COO^-]_F}{[NH_3^+]_F}$ now varies respectively between 0.7 and 2 (Table 2).

Within the hypothesis of a contained ionic strength (this point will be discussed at the end of the manuscript), the formation of *MLWV* occurs just above pH 7, in the proximity of, or slightly above, the pKa of oleic acid, with a $\frac{[COO^-]_F}{[NH_3^+]_F}$ content ranging between 2 and 5. *MLWV* are then stable until pH 4, when $\frac{[COO^-]_F}{[NH_3^+]_F}$ falls below the range 0.5 – 1. Finally, in terms of amount of lipid and PLL consumed, NMR shows that an average of about 70% of the initial content of G-C18:1 is employed to form *MLWV* in spite of less than 10% of the initial PLL content. Variations in the initial $\frac{[\mathrm{G-C18{:}1}]_{In}}{[\mathrm{PLL}]_{In}}$ do not seem to have any particular influence on the amount of consumed reactants.

Table 2 – Quantitative evaluation of G-C18:1 and PLL in *MLWV* by ^{1}H solution NMR. The NMR spectra and full list of parameters are respectively given in Figure S 11 and Table S 1. In brief: the molar ratio column gives the G-C18:1-to-PLL molar ratio (square brackets identify molar concentrations) in the initial solution ($\frac{[\mathrm{G-C18{:}1}]_{In}}{[\mathrm{PLL}]_{In}}$) and in the *MLWV* phase ($\frac{[\mathrm{G-C18{:}1}]_{F}}{[\mathrm{PLL}]_{F}}$). The monomer ratio column identifies the ratio

between the neutral $\frac{[COOH]_F}{[NH_2]_F}$ and charged $\frac{[COO^-]_F}{[NH_3^+]_F}$ functional groups in the *MLWV*. $\frac{[COO^-]_F}{[NH_3^+]_F}$ is calculated from $\frac{[COOH]_F}{[NH_2]_F}$ assuming that the interaction occurs at pH 5, with 100 % of NH_3^+ and two values of COO^- (10% and 30%), estimated at the same pH for a pKa of about 7. The % consumed column identifies the molar percentage of consumed G-C18:1 and PLL during formation of *MLWV* (subscript *F*) with respect to their initial concentration (subscript *In*) in solution.

Molar ratio		Monomer ratio in *MLWV*			% consumed reactants in *MLWV*	
$\frac{[\mathrm{G-C18:1}]_{In}}{[\mathrm{PLL}]_{In}}$ *(in solution)*	$\frac{[\mathrm{G-C18:1}]_F}{[\mathrm{PLL}]_F}$ *(in MLWV)*	$\frac{[COOH]_F}{[NH_2]_F}$	$\frac{[COO^-]_F}{[NH_3^+]_F}$		$\frac{[\mathrm{G-C18:1}]_F}{[\mathrm{G-C18:1}]_{In}}$	$\frac{[\mathrm{PLL}]_F}{[\mathrm{PLL}]_{In}}$
			(10% COO^-)	(30% COO^-)		
5.4	92 ± 22	4.6 ± 1.1	0.5 ± 0.1	1.4 ± 0.3	63 ± 11	3.7 ± 0.6
10.8	192 ± 46	9.6 ± 2.3	1.0 ± 0.2	2.9 ± 0.7	69 ± 12	3.9 ± 0.7
21.6	144 ± 35	7.2 ± 1.7	0.7 ± 0.2	2.2 ± 0.5	47 ± 8	7.0 ± 1.2
2.75	113 ± 27	5.7 ± 1.4	0.6 ± 0.1	1.7 ± 0.4	94 ± 16	2.3 ± 0.4

To confirm and strengthen the NMR data, ITC experiments are performed in the *MLWV* phase region. In particular, ITC provides a direct proof of the specificity of the interaction between G-C18:1 and PLL and it quantifies its thermodynamic parameters. Figure 7a shows the heat rate profile upon controlled injections of buffer (phosphate) and G-C18:1 solutions into a PLL solution. The negative peaks identify an exothermic process, while the rapid loss in the heat rate intensity, compared to the buffer injection, shows that PLL binding sites are rapidly saturated with G-C18:1. Typically, data obtained by ITC for the adsorption of surfactant on polyelectrolytes are interpreted by using the Satake-Yang binding isotherm,[93] but more recent multiple site binding models have appeared in the literature[94,95] and are provided by the Nanoanalyze software,[96] allowing a handy way to extract thermodynamic parameters and to compare them across studies.[97,98] The "independent model" considers the interaction of "n" ligands with a macromolecule that has one binding site (or multiple equivalent binding sites);[99,100,101] the "multiple site" model allows for fitting to two independent sites, each with a unique association constant, k_a, stoichiometry, n, and enthalpy change, ΔH; the "sequential (two sites)" model considers two binding sites where the first is populated before the second accepts a ligand.

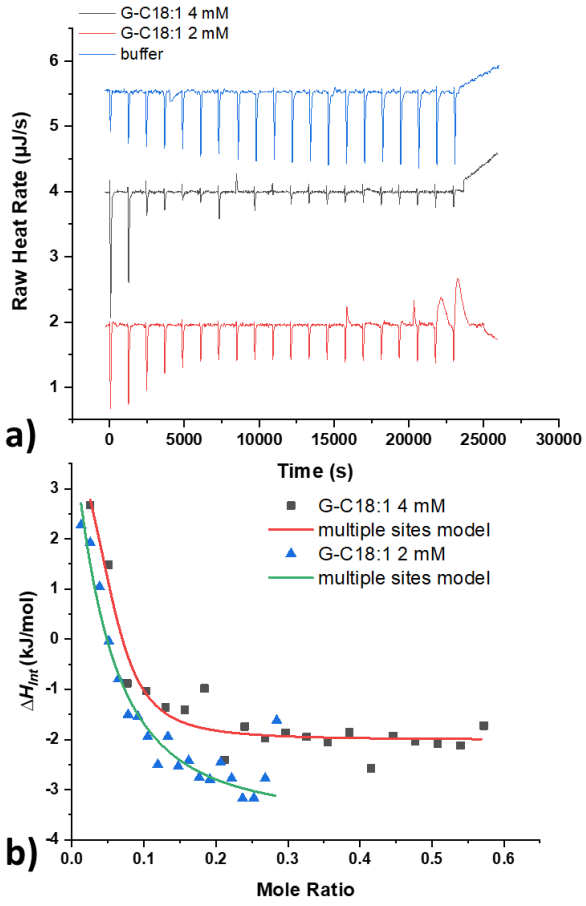

Figure 7 - a) ITC heat rate profiles of buffer (blue) and G-C18:1 (C= 4 mM, black; C= 2 mM, red) solutions injected into a PLL solution (C= 2 mM). b) Evolution of the ΔH_{Int} (= $\Delta H_{G-C18:1/PLL}$-ΔH_{Buffer}) with PLL/G-C18:1 molar ratio derived from (a). The fit is performed with a "multiple site" model provided by the Nanoanalyze software.

In this work, the independent model is not able to fit the data and it is then discarded. The evolution of the enthalpy change of interaction, ΔH_{Int}, with mole ratio (Figure 7b) can be satisfactorily fitted with both the "multiple site" and "sequential (two sites)" models. However, one should be aware of the fact Langmuir-type binding isotherms do make some assumptions which are not completely satisfied for the experiments and results should be interpreted with caution and with an eye on the underlying physics. Here, the highest consistency between the fitting results and the physics of adsorption of G-C18:1 onto PLL is obtained with the "multiple site" model, interpreted hereafter.

The thermodynamic parameters extracted from the fit of the enthalpy profile are given in Table 3. The first interaction has a positive enthalpy change (ΔH_1= 28.9 ± 0.9 kJ/mol) and an entropy variation of $T\Delta S_1$= 76.7 ± 22.8 kJ/mol. The second interaction shows a negative

entropy change (ΔH_2= -2.8 ± 0.8 kJ/mol) and a smaller entropy variation ($T\Delta S_2$= 33.6 ± 1.1 kJ/mol). Please note that the denominations first and second do not specify sequential interactions, i.e. they can occur in any random order, as both sites are independent. These data illustrate that the first interaction is endothermic, non-specific and essentially entropy-dependent, most likely driven by the hydrophobic effect. On the contrary, the second is exothermic, specific and most likely driven by electrostatic and/or of H-bonding interactions,[98] as also found for β-lactoglobulin/sodium alginate in the pH range where they are oppositely charged.[102] Both interactions are of equivalent importance for the association of G-C18:1 and PLL, considering that both Gibbs free energies (ΔG) are negative and of the same order of magnitude.

From a mechanistic point of view, we interpret these data with a standard surfactant-polyelectrolyte approach:[98] G-C18:1 strongly binds to PPL through specific interactions (ΔH_2< 0) with an entropic ($T\Delta S_2$> 0) component, most likely coming from the release of water and counterions initially associated to the charged binding sites. The stoichiometry of the interaction in Table 3 corresponds to the monomer stoichiometry, also evaluated by NMR in Table 2 ($n_2 \equiv \frac{[COOH]_F}{[NH_2]_F}$). ITC provides n_2= 3.8 ± 0.7 with an affinity of K_{a2}= 2.62 ± 1.48 $\cdot 10^6$ M^{-1}, where n_2 is in very good agreement, within the error, with $<\frac{[COOH]_F}{[NH_2]_F}>$= 6.8 ± 2.2, the average monomer ratio found by NMR. ITC and NMR experiments are performed under different experimental and sample preparation conditions; the agreement between n_2 and $\frac{[COOH]_F}{[NH_2]_F}$ strongly support the reliability of the hypothesis formulated in Figure 6. The order of magnitude of the interactions and affinity constants found here are in also good agreement with the values published in the literature for similar systems, where $|\Delta H|$ varies between 1 and 20 kJ/mol, $|T\Delta S|$ between 1 and 50 kJ/mol with affinity constants in the order of 10^7 M^{-1}.[97,103–105]

The second energetic contribution found in the [G-C18:1+PLL] system is non-specific (ΔH_2> 0) and it corresponds to the clustering, or grouping, of the non-polar tails of G-C18:1 molecules, driven by the release of water ($T\Delta S_2$> 0). Similar coexisting specific and non-specific interactions were reported in hyaluronan/cationic vesicles system[106] or gum acacia/bovine serum albumin system[107] and are well-known in polyelectrolyte-micelle coacervation ("polymer-driven micellization").[98]

Table 3 - Thermodynamic parameters extracted from fitted data in Figure 7b using a "multiple site" model at T= 298 K. Data are averaged for the two experiments, of which the corresponding parameters of the fits are given in the Supporting Information (Table S 2 and Table S 3). k_a is the association constant, n is the

G-C18:1 to PLL monomer stoichiometry ($\equiv \frac{[COOH]_F}{[NH_2]_F}$) and ΔH, ΔG and ΔS are respectively the enthalpy, Gibbs' free energy and entropy change.

Interaction type	Parameter	Value
Non-specific Endothermic (entropic, hydrophobic effect)	K_{a1}	$2.4 \pm 0.8 \cdot 10^8$ M^{-1}
	n_1	0.03 ± 0.02
	ΔG_1	-47.7 ± 1.2 kJ/mol
	ΔH_1	28.9 ± 0.9 kJ/mol
	ΔS_1	0.3 ± 0.1 kJ/mol·K
Specific Exothermic (electrostatic, H-bonding)	K_{a2}	$2.6 \pm 1.5 \cdot 10^6$ M^{-1}
	n_2	3.8 ± 0.7
	ΔG_2	-36.4 ± 1.9 kJ/mol
	ΔH_2	-2.8 ± 0.8 kJ/mol
	ΔS_2	0.10 ± 0.04 kJ/mol·K

Discussion

Figure 8 summarizes the major findings of this work. SL-C18:0 is a lipid which undergoes a direct micelle-to-fiber transition in water in the vicinity of pH 7. We had proposed a nucleation and growth mechanism of the fibers with no apparent structural continuity with the micelles, which act as reservoir of matter.[49,59] In the presence of a polyelectrolyte, such mechanism persists. Above pH 7.5, the negatively-charged micelles are complexed by the polyelectrolyte into a complex coacervate (*Co* phase), of which we find two major structures by cryo-TEM, a dense cluster of micelles (panel 1 in Figure 3) coexisting with a PLL-rich (*sc* in Figure 3) and textured, "pearl-necklace"-like, glycolipid-rich medium (panels 2,3 in Figure 3). Below pH 7.5, the coacervate phase disassembles in favour of a twisted ribbon phase, only composed of SL-C18:0 only, as confirmed by ^{1}H solution NMR experiments (Figure S 11c,d). Interestingly, ribbons were shown to form by the interaction of bile salts with block copolymers,[46] and for this reason we speculate that SL-C18:0 fibers are either neutral objects of their surface charge is too low for complexation to occur. We stress however the fact that at the moment we do not have a direct measurement of the fibers' surface charge. As in the PEC-free system, the coacervate-to-fiber transition occurs in less than a pH unit and without any intermediate. This general mechanism is shown in Figure 8a. The best hypothesis, to be eventually verified with other complementary techniques, is that upon charge compensation during lowering pH, SL-C18:0 molecules are progressively acidified and slowly diffuse from the micellar environment to the solution. The solubility of acidic SL-C18:0 in water is low and

for this reason, after reaching a critical concentration, nucleation of the twisted ribbons occurs, followed by growth and concomitant disruption of the coacervate. Last but not least, the nature of the PEC has no influence on the coacervate-to-fiber transition, indicating that PEC rigidity and charge density play no significant role.

In the absence of a polyelectrolyte, G-C18:1 undergoes a micelle-to-vesicle-to-lamellar phase transition, characterized by a structural and morphological continuity.[49] In the presence of PLL (generalization to other PEC is presented elsewhere),[64] G-C18:1 forms a *Co* phase in the micelle region of its phase diagram at pH> 7. If combination of cryo-TEM and SAXS suggests a textured worm-like structure of the coacervate (Figure 3d) rather than a "pearl-necklace" , complexation by the polyelectrolyte does not induce shape transition in the G-C18:1 micelles. This is in line with the body of data published on surfactant-polyelectrolyte coacervates[21] and probably explained by the low binding affinity of ammonium groups.[108] Below approximately pH 7.5, we find a transition between the complex coacervate and multilamellar walls vesicles. This is driven by an isostructural and isodimensional (Figure 6c,d) micelle-to-membrane transition (Figure 6a,b): the diameter of the micelles, embedded in the coacervate phase, is equivalent to the thickness of the membrane. The thickness corresponds to the length of a single G-C18:1 molecule (Figure 6d), as previously found for this systems[49] and expected for bolaamphiphiles.[71] *MLWV* are stable in the pH interval between 7 and 5. A decrease in pH corresponds to an increasing content of the acidic form of G-C18:1 in the membrane and a consequent lowering of the membrane charge density. For this reason, the interlamellar distance increases by decreasing pH, due to the increasing thickness of PLL, hence causing an increase in repulsive pressure, upon lowering the charge density of the membrane (Figure 6e).[74] Quantitative ^{1}H NMR experiments confirm that *MLWV* are composed of both G-C18:1 and PLL with an average monomer stoichiometry of 6.8 ± 2.2. Considerations about the pKa (here assumed to be about 7) and pH at which MLWV are prepared (5) suggest a situation of charge compensation between carboxylic acids and ammonium groups. Such specific interactions (ΔH_2= -2.8 ± 0.8 kJ/mol) with a comparable stoichiometry (3.8 ± 0.7) and high affinity (K_{a2}= 2.6 ± 1.5 $\cdot 10^6$ M^{-1}) are also confirmed by independent ITC experiments. When the amount of negative charges has lowered at a point below which attractive interaction with PLL can no longer hold the membranes together (between pH 5 and pH 4), *MLWV* experience a loss in the long-range lamellar order. This is followed by the complete disruption of the *MLWV*, causing the expulsion of PLL and eventually followed, below pH 3, by precipitation of a polyelectrolyte-free lamellar phase only composed of G-C18:1 (Figure 6e and Figure 8b). If pH is increased again, *MLWV* form again in their pH stability range. However, further increase

in pH does not induce a reversed *MLWV*-to-*Co* transition, but rather the formation of free micelles and PLL.

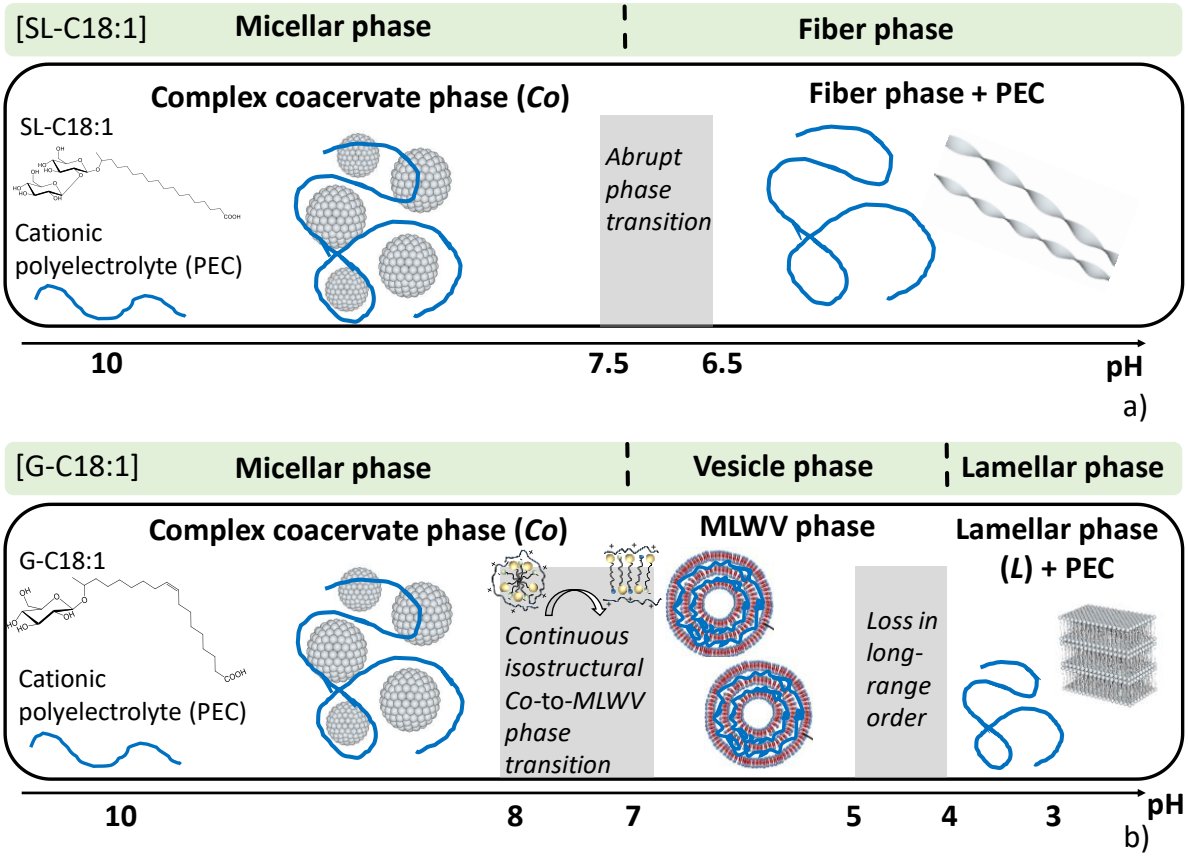

Figure 8 – Summary of the pH-driven phase transitions of (a) SL-C18:0 and (b) G-C18:1 lipids alone and in the presence of PLL polyelectrolyte in water at room temperature and *C*< 1 wt%.

Our data show that the *Co*-to-*MLWV* transition is driven by the dynamic variation in the effective packing parameter of G-C18:1 and which depends on the transition from its ionic to neutral form. If this result is coherent with previous studies on the equilibrium phase diagrams of PECSs, where the packing parameter of the PESC was modified either by using a cosurfactant[6,24] or by varying the nature of the polar headgroup,[35] we do not find a major influence of the type of polyelectrolyte, as proposed elsewhere.[7] This is unexpected, especially considering the strong impact of polyelectrolytes on the membrane bending energy already discussed above. It has been recently shown that the pH-driven micelle-to-vesicle transition in free ethoxy fatty acids solutions[34] can be inhibited in the presence of a polyelectrolyte.[35] In fact, to the best of our knowledge, evidence of isostructural and isodimensional micelle-to-vesicle transition in PESCs at concentrations as low as 0.2 wt% have hardly been described. Lamellar or multilamellar PESCs phases are far from being uncommon but they are generally obtained

for calibrated formulations[35] and often at high lipid concentrations (generally above 10 wt%).[24] Furthermore, similar phase transitions were never reported in specific polyelectrolyte-surfactant complex coacervate systems.

It is worth mentioning a short comment on the *MLWV* structure, which we systematically find, instead of flat lamellar phase or agglutinated single-wall vesicles. We have discussed the former situation as the overwhelming effect of the intrinsic bending energy of the G-C18:1 interdigitated layered membrane overwhelming the competing structuring effect of the polyelectrolyte. Although we cannot quantify it, it seems clear that any of the polyelectrolytes employed in this study are neither rigid enough nor bind strongly enough to generate a flat membrane.

Whether the non-equilibrium continuous pH variation to cross the micelle-vesicle boundary of G-C18:1 has any impact on the *Co*-to-*MLWV* transition is an open question to which we can answer only partially. Vesicles are generally considered as metastable structures, although in some cases, when the structure does not evolve for an "infinitely" long time, they are assumed to be at equilibrium. G-C18:1 spontaneously self-assembles into vesicles upon pH variation from alkaline to acidic pH under conditions of both pseudo-[54] and non-equilibrium (Figure 5a).[49] Furthermore, unpublished in-lab tests show that G-C18:1 in fact spontaneously forms vesicles by a simple dispersion in water at pH below 7 and by application of moderate amounts of energy (e.g., bath sonication). G-C18:1 vesicles tend to be colloidally stable over long periods of time (months). On the basis of these observation, one can qualitatively say that the vesicle phase is the thermodynamic phase of G-C18:1 under acidic pH conditions. Given the above, MLWV structures should be systematically obtained if pH is varied extremely slow or if a G-C18:1 pre-formed vesicles and PEC solutions are mixed at acidic pH. In the first approach, it would be hard and ridiculously long to determine which rate of pH variation would be considered to be compatible with equilibrium conditions. For instance, Chiappisi *et al*. have employed equilibration times for a given pH value between 2 and 15 days.[35,68] For this reason, we have employed the second approach, reported elsewhere,[64] and which does not show the formation of a single MLWV phase but rather a multiphasic system composed of agglutinated vesicles, cabbage-like structure and MLWV.

Agglutination of single-wall vesicles (SWV)[25,109,110] against the formation of *MLWV* is an open, and important, question in the literature both from a fundamental[110] and applicative points of view, as agglutination is important in the field of life science,[110] while *MLWV* have a specific interest in gene transfection applications.[111] If several authors have explained the origin of *MLWV* structures as a simple matter of lipid-to-polyelectrolyte ratio,[3,111,112] other authors

show contradictory data, where a mixture of both can be found.[113] In the present system, we rather believe that the systematic production of *MLWV*, instead of agglutinated SWV, depends on the combination between the pre-existing complex coacervate phase, inside which the isostructural and isodimensional micelle-to-vesicle phase transition occurs, and the non-equilibrium pH variation, which traps the system in the MLWV phase. Separation between these mechanisms is shown elsewhere.[64]

Finally, the *Co*-to-*MLWV* transition is driven by a pH jump process, meaning that salt is continuously generated. Ionic strength is an important parameter with a strong impact on the stability of PESCs, but the charge density on both the polymer and the colloid, equally pH-dependent, are also very important for the PESC stability.[21] Under the experimental conditions of this work, the amount of generated salt is in the order of 50 mM. Such concentration is modest compared to other studied reaching ionic strength as high as 0.4 M,[62] but it could play a role in the overall electroneutrality and charge stoichiometry of both coacervates and *MLWV*. However, the pH jump process, necessary to drive the *Co*-to-*MLWV* transition, does not prevent the formation of both the *Co* and *MLWV* phases. Even if preliminary data (not displayed here) seem to show that MLWV are stable up to 0.5 M NaCl, we suspect salt to be responsible for the lack of reversibility of the Co-to-MLWV-to-Co transition (Figure S 10), meaning that this parameter certainly deserves to be studied in detail in relationship to the stability of PESCs containing G-C18:1.

Conclusion

Non-equilibrium phase transitions in polyelectrolyte-surfactant complex (PESC) coacervates (*Co*) are addressed in this work by mean of stimuli-responsive negatively-charged amphiphiles and cationic polyelectrolytes. We employ two microbial glycolipid biosurfactants known to undergo micelle-to-fiber (deacetylated acidic C18:0 sophorolipids, SL-C18:0) and micelle-to-vesicle (deacetylated acidic C18:1 glucolipids, G-C18:1) phase transition when pH is lowered from alkaline to acidic. In the alkaline pH domain, both amphiphiles mainly form a phase characterized by negatively-charged micelles. Upon mixing with a positively-charged polyelectrolyte, pH-resolved *in situ* SAXS, DLS and ζ-potential combined with cryo-TEM show the formation of globally neutral PESC polyelectrolyte-surfactant coacervates. Upon acidification of the solution, the SL-C18:0 amphiphile undergoes a micelle-to-fiber transition, independently from the presence of the polyelectrolyte, which, according to ^{1}H NMR arguments, is most likely released in solution and it coexists with the fibers, but without specific interactions, differently than other similar systems.[46] The micelle-to-fiber transition is hence

responsible for the disruption of the complex coacervate, which becomes unstable below pH ~7, the transition pH of the SL-C18:0 surfactant alone.

At the micelle-vesicle boundary, we find a continuous isostructural and isodimensional transition between complex coacervate (*Co*) and multilamellar wall vesicles (*MLWV*). By reducing the negative charge density during acidification, the micellar aggregates embedded in the *Co* phase are characterized by a decrease in the local curvature, which drives the transition from spheres to membranes, composed of interdigitated G-C18:1 molecules. The residual negative charge density guarantees electrostatic interaction with the polyelectrolyte, which keeps the membranes together. This is supported by both NMR and ITC experiments, providing a comparable charge stoichiometry and the latter showing specific interactions ($\Delta H < 0$). The bending energy associated to the polyelectrolyte-membrane complex is low enough for the lipid membrane to bend and drive the formation of vesicular colloids, characterized by multilamellar walls. The membrane thickness is equivalent to the micellar radius and compatible with the length of G-C18:1, testifying the isostructural and isodimensional transition. At lower pH, the membrane charge density becomes low and interactions with the polyelectrolyte less strong. This phenomenon promotes intra-chain electrostatic repulsion interactions and eventual swelling of the lamellar region. Finally, when the membrane becomes neutral, polymeric repulsion becomes strong enough to disassemble the lamellae. The polyelectrolyte will most likely be entirely solvated and at sufficiently low pH (< 3) the G-C18:1 precipitated in the form of a poorly-ordered, polyelectrolyte-free, lamellar phase, as found in the control lipid solution at the same pH. Upon increasing pH, *MLWV* form again but we do not find reversibility in the *MLWV*-to-*Co* transition.

This work shows that surfactant phase transitions driven by a non-equilibrium pH variation drive the complex coacervate out of its stability region. This occurs either through the loss of the polyelectrolyte-surfactant aggregation or through the formation of a new complex phase. In both cases, the nature of the polyelectrolyte (e.g., rigidity or charge density) does not have any significant influence on the fate of the transition, as found for most PESCs. For the *MLWV* phase, the bending energy of the lipid membrane is low enough to counterbalance the strong adsorption and stiffness of the polyelectrolyte, which could otherwise drive the formation of a flat lamellar phase. At the same time, combination between the isostructural and isodimensional transition occurring in the confined micellar complex coacervate with non-equilibrium pH variation drive the formation of a *MLWV* phase, interesting for biomedical applications, rather than of a system composed of agglutinated single-wall vesicles, as found in many other systems. Finally, we stress the fact that this work demonstrates the possibility to

prepare a new generation of stimuli-responsive and fully sustainable PESCs due to the use of biosurfactants.

Acknowledgements

Diamond synchrotron radiation facility (U. K.) is acknowledged for accessing to the B21 beamline and financial support (proposal N° 23247). Ghazi Ben Messaoud (DWI-Leibniz Institute for Interactive Materials, Aachen, Germany) is kindly acknowledged for helpful discussions. We thank Dr. S. Roelants, Prof. W. Soetaert and Prof. C. V. Stevens at Gent University for providing us the glycolipids. We thank P. Dhasaiyan (Institute for Basic Science Center for Self Assembly and Complexity, Gyeongsangbuk-do, South Korea) for helpful suggestions. This work benefited from the use of the SasView application, originally developed under NSF award DMR-0520547. SasView containscode developedwith funding from the European Union's Horizon 2020 research and innovation program under the SINE2020project, grant agreement No. 654000. WT and GK acknowledge financial support from KU Leuven (grants C14/18/061 and IDN/19/014) and Research Foundation - Flanders (grant G.0C60.13N). Soleil Synchrotron facility for accessing the Swing beamline and financial support (proposal N° 20190961). Sorbonne Université (contract N°3083/2018) is acknowledged for financial support of CS. The authors acknowledge the French ANR for financial support, project N° SELFAMPHI - 19-CE43-0012-01.

Supporting Information: Figure S1 to Figure S11, Table S1 to Table S3, explicative text.

References

(1) Kronberg, B.; Holmberg, K.; Lindman, B. *Surface Chemistry of Surfactants and Polymers*; John Wiley & Sons, Inc., 2014.

(2) *Dna Interactions With Polymers and Surfactants*; Dias, R., Lindman, B., Eds.; John Wiley & Sons, Inc.: Hoboken, New Jersey, 2008.

(3) Gradzielski, M.; Hoffmann, I. Polyelectrolyte-Surfactant Complexes (PESCs) Composed of Oppositely Charged Components. *Curr. Opin. Colloid Interface Sci.* **2018**, *35*, 124–141.

(4) Ferreira, G. A.; Loh, W. Liquid Crystalline Nanoparticles Formed by Oppositely Charged Surfactant-Polyelectrolyte Complexes. *Curr. Opin. Colloid Interface Sci.* **2017**, *32*, 11–22.

(5) Lindman, B.; Antunes, F.; Aidarova, S.; Miguel, M.; Nylander, T. Polyelectrolyte-

Surfactant Association—from Fundamentals to Applications. *Colloid J.* **2014**, *76*, 585–594.

(6) Piculell, L. Understanding and Exploiting the Phase Behavior of Mixtures of Oppositely Charged Polymers and Surfactants in Water. *Langmuir* **2013**, *29*, 10313–10329.

(7) Chiappisi, L.; Hoffmann, I.; Gradzielski, M. Complexes of Oppositely Charged Polyelectrolytes and Surfactants - Recent Developments in the Field of Biologically Derived Polyelectrolytes. *Soft Matter* **2013**, *9*, 3896–3909.

(8) Schmitt, C.; Turgeon, S. L. Protein/Polysaccharide Complexes and Coacervates in Food Systems. *Adv. Colloid Interface Sci.* **2011**, *167*, 63–70.

(9) Winslow, B. D.; Shao, H.; Stewart, R. J.; Tresco, P. A. Biocompatibility of Adhesive Complex Coacervates Modeled after the Sandcastle Glue of Phragmatopoma Californica for Craniofacial Reconstruction. *Biomaterials* **2010**, *31*, 9373–9381.

(10) Johnson, N. R.; Wang, Y. Coacervate Delivery Systems for Proteins and Small Molecule Drugs. *Expert Opin. Drug Deliv.* **2014**, *11*, 1829–1832.

(11) Hwang, D. S.; Zeng, H.; Srivastava, A.; Krogstad, D. V.; Tirrell, M.; Israelachvili, J. N.; Waite, J. H. Viscosity and Interfacial Properties in a Mussel-Inspired Adhesive Coacervate. *Soft Matter* **2010**, *6*, 3232–3236.

(12) Baccile, N.; Reboul, J.; Blanc, B.; Coq, B.; Lacroix-Desmazes, P.; In, M.; Gérardin, C. Ecodesign of Ordered Mesoporous Materials Obtained with Switchable Micellar Assemblies. *Angew. Chemie - Int. Ed.* **2008**, *47*, 8433–8437.

(13) Chiappisi, L.; Simon, M.; Gradzielski, M. Toward Bioderived Intelligent Nanocarriers for Controlled Pollutant Recovery and PH-Sensitive Binding. *ACS Appl. Mater. Interfaces* **2015**, *7*, 6139–6145.

(14) Hiwatari, Y.; Yoshida, K.; Akutsu, T.; Yabu, M.; Iwai, S. Polyelectrolyte-Micelle Coacervation: Effect of Coacervate on the Properties of Shampoo. *J. Soc. Cosmet. Chem. Japan* **2004**, *26*, 315–316.

(15) Burgess, D. J.; Ponsart, S. B-Glucuronidase Activity Following Complex Coacervation and Spray Drying Microencapsulation. *J. Microencapsul.* **1998**, *15*, 569–579.

(16) Wang, Y. F.; Gao, J. Y.; Dubin, P. L. Protein Separation via Polyelectrolyte Coacervation: Selectivity and Efficiency. *Biotechnol. Prog.* **1996**, *12*, 356–362.

(17) Jones, O. G.; Lesmes, U.; Dubin, P.; McClements, D. J. Effect of Polysaccharide Charge on Formation and Properties of Biopolymer Nanoparticles Created by Heat Treatment of β-Lactoglobulin-Pectin Complexes. *Food Hydrocoll.* **2010**, *24*, 374–383.

(18) Israelachvili, J. N.; Mitchell, D. J.; Ninham, B. W. Theory of Self-Assembly of Hydrocarbon Amphiphiles into Micelles and Bilayers. *J. Chem. Soc. Faraday Trans. 2* **1976**, *72*, 1525.

(19) Bilalov, A.; Olsson, U.; Lindman, B. Complexation between DNA and Surfactants and Lipids: Phase Behavior and Molecular Organization. *Soft Matter* **2012**, *8*, 11022–11033.

(20) Kogej, K. Association and Structure Formation in Oppositely Charged Polyelectrolyte-Surfactant Mixtures. *Adv. Colloid Interface Sci.* **2010**, *158*, 68–83.

(21) Kizilay, E.; Kayitmazer, A. B.; Dubin, P. L. Complexation and Coacervation of Polyelectrolytes with Oppositely Charged Colloids. *Adv. Colloid Interface Sci.* **2011**, *167*, 24–37.

(22) Sing, C. E.; Perry, S. L. Recent Progress in the Science of Complex Coacervation. *Soft Matter* **2020**, *16*, 2885–2914.

(23) Kizilay, E.; Dinsmore, A. D.; Hoagland, D. A.; Sun, L.; Dubin, P. L. Evolution of Hierarchical Structures in Polyelectrolyte-Micelle Coacervates. *Soft Matter* **2013**, *9*, 7320–7332.

(24) Piculell, L.; Norrman, J.; Svensson, A. V.; Lynch, I.; Bernardes, J. S.; Loh, W. Ionic Surfactants with Polymeric Counterions. *Adv. Colloid Interface Sci.* **2009**, *147–148*, 228–236.

(25) Antunes, F. E.; Marques, E. F.; Miguel, M. G.; Lindman, B. Polymer-Vesicle Association. *Adv. Colloid Interface Sci.* **2009**, *147–148*, 18–35.

(26) Stanic, V.; Mancuso, M.; Wong, W.; Dimasi, E.; Strey, H. H. Phase Diagrams of Electrostatically Self-Assembled Amphiplexes. *Macromolecules* **2011**, *44*, 7423–7429.

(27) Mekhloufi, G.; Sanchez, C.; Renard, D.; Guillemin, S.; Hardy, J. PH-Induced Structural Transitions during Complexation and Coacervation of β-Lactoglobulin and Acacia Gum. *Langmuir* **2005**, *21*, 386–394.

(28) Rawat, K.; Aswal, V. K.; Bohidar, H. B. DNA-Gelatin Complex Coacervation, UCST and First-Order Phase Transition of Coacervate to Anisotropic Ion Gel in 1-Methyl-3-Octylimidazolium Chloride Ionic Liquid Solutions. *J. Phys. Chem. B* **2012**, *116*, 14805–14816.

(29) Vieregg, J. R.; Lueckheide, M.; Marciel, A. B.; Leon, L.; Bologna, A. J.; Rivera, J. R.; Tirrell, M. V. Oligonucleotide-Peptide Complexes: Phase Control by Hybridization. *J. Am. Chem. Soc.* **2018**, *140*, 1632–1638.

(30) Love, C.; Steinkühler, J.; Gonzales, D. T.; Yandrapalli, N.; Robinson, T.; Dimova, R.;

Tang, T. Y. D. Reversible PH-Responsive Coacervate Formation in Lipid Vesicles Activates Dormant Enzymatic Reactions. *Angew. Chemie - Int. Ed.* **2020**, *59*, 5950–5957.

(31) Last, M. G. F.; Deshpande, S.; Dekker, C. PH-Controlled Coacervate-Membrane Interactions within Liposomes. *ACS Nano* **2020**, 10.1021/acsnano.9b10167.

(32) Lasic, D. D. *Liposomes: From Physics to Applications*; Elsevier, Ed.; 1993.

(33) Leng, J.; Egelhaaf, S. U.; Cates, M. E. Kinetics of the Micelle-to-Vesicle Transition: Aqueous Lecithin-Bile Salt Mixtures. *Biophys. J. Vol.* **2003**, *85*, 1624–1646.

(34) Hayward, D. W.; Chiappisi, L.; Teo, J. H.; Prévost, S.; Schweins, R.; Gradzielski, M. Neutralisation Rate Controls the Self-Assembly of PH-Sensitive Surfactants. *Soft Matter* **2019**, *15*, 8611–8620.

(35) Chiappisi, L.; Prévost, S.; Grillo, I.; Gradzielski, M. From Crab Shells to Smart Systems: Chitosan-Alkylethoxy Carboxylate Complexes. *Langmuir* **2014**, *30*, 10615–10616.

(36) Brooks, J. T.; Marques, C. M.; Cates, M. E. The Effect of Adsorbed Polymer on the Elastic Moduli of Surfactant Bilayers. *J. Phys. II* **1991**, *1*, 673–690.

(37) Harries, D.; Ben-Shaul, A.; Szleifer, I. Enveloping of Charged Proteins by Lipid Bilayers. *J. Phys. Chem. B* **2004**, *108*, 1491–1496.

(38) May, S.; Ben-Shaul, A. DNA-Lipid Complexes: Stability of Honeycomb-like and Spaghetti-like Structures. *Biophys. J.* **1997**, *73*, 2427–2440.

(39) May, S. Stability of Macroion-Decorated Lipid Membranes. *J. Phys. Condens. Matter* **2005**, *17*.

(40) Sjöström, L.; Åkesson, T.; Jönsson, B. Interaction and Conformation of Polyelectrolyte Chains Adsorbed on Neutral Surfaces. *J. Chem. Phys.* **1993**, *99*, 4739–4747.

(41) Fleer, G. J.; Stuart, M. A. C.; Scheutjens, J. M. H. M.; Cosgrove, T.; Vincent, B. *Polymers at Interfaces*, 1998th ed.; Springer-Science, 1998.

(42) Wang, J.; Guo, K.; Qiu, F.; Zhang, H.; Yang, Y. Predicting Shapes of Polymer-Chain-Anchored Fluid Vesicles. *Phys. Rev. E - Stat. Nonlinear, Soft Matter Phys.* **2005**, *71*, 1–5.

(43) Li, D.; Wagner, N. J. Universal Binding Behavior for Ionic Alkyl Surfactants with Oppositely Charged Polyelectrolytes. *J. Am. Chem. Soc.* **2013**, *135*, 17547–17555.

(44) Okesola, B. O.; Smith, D. K. Applying Low-Molecular Weight Supramolecular Gelators in an Environmental Setting-Self-Assembled Gels as Smart Materials for Pollutant Removal. *Chem. Soc. Rev.* **2016**, *45*, 4226–4251.

(45) Liu, X. Y.; Sawant, P. D. Formation Kinetics of Fractal Nanofiber Networks in Organogels. *Appl. Phys. Lett.* **2001**, *79*, 3518–3520.

(46) Di Gregorio, M. C.; Gubitosi, M.; Travaglini, L.; Pavel, N. V.; Jover, A.; Meijide, F.; Vázquez Tato, J.; Sennato, S.; Schillén, K.; Tranchini, F.; et al. Supramolecular Assembly of a Thermoresponsive Steroidal Surfactant with an Oppositely Charged Thermoresponsive Block Copolymer. *Phys. Chem. Chem. Phys.* **2017**, *19*, 1504–1515.

(47) Dhasaiyan, P.; Prasad, B. L. V. Self-Assembly of Bolaamphiphilic Molecules. *Chem. Rec.* **2017**, *17*, 597–610.

(48) Kitamoto, D.; Morita, T.; Fukuoka, T.; Konishi, M.; Imura, T. Self-Assembling Properties of Glycolipid Biosurfactants and Their Potential Applications. *Curr. Op. Coll. Interf. Sci.* **2009**, *14*, 315–328.

(49) Baccile, N.; Cuvier, A.-S.; Prévost, S.; Stevens, C. V.; Delbeke, E.; Berton, J.; Soetaert, W.; Van Bogaert, I. N. A.; Roelants, S. Self-Assembly Mechanism of PH-Responsive Glycolipids: Micelles, Fibers, Vesicles, and Bilayers. *Langmuir* **2016**, *32*, 10881–10894.

(50) Palareti, G.; Legnani, C.; Cosmi, B.; Antonucci, E.; Erba, N.; Poli, D.; Testa, S.; Tosetto, A. Comparison between Different D-Dimer Cutoff Values to Assess the Individual Risk of Recurrent Venous Thromboembolism: Analysis of Results Obtained in the DULCIS Study. *Int. J. Lab. Hematol.* **2016**, *38*, 42–49.

(51) Baccile, N.; Pedersen, J. S.; Pehau-Arnaudet, G.; Van Bogaert, I. N. a. Surface Charge of Acidic Sophorolipid Micelles: Effect of Base and Time. *Soft Matter* **2013**, *9*, 4911–4922.

(52) Baccile, N.; Babonneau, F.; Jestin, J.; Pehau-Arnaudet, G.; Van Bogaert, I. Unusual, PH-Induced, Self-Assembly of Sophorolipid Biosurfactants. *ACS Nano* **2012**, *6*, 4763–4776.

(53) Ben Messaoud, G.; Promeneur, L.; Brennich, M.; Roelants, S. L. K. W.; Le Griel, P.; Baccile, N. Complex Coacervation of Natural Sophorolipid Bolaamphiphile Micelles with Cationic Polyelectrolytes. *Green Chem.* **2018**, *20*, 3371–3385.

(54) Baccile, N.; Selmane, M.; Le Griel, P.; Prévost, S.; Perez, J.; Stevens, C. V.; Delbeke, E.; Zibek, S.; Guenther, M.; Soetaert, W.; et al. PH-Driven Self-Assembly of Acidic Microbial Glycolipids. *Langmuir* **2016**.

(55) Cuvier, A. S.; Berton, J.; Stevens, C. V.; Fadda, G. C.; Babonneau, F.; Van Bogaert, I. N. A.; Soetaert, W.; Pehau-Arnaudet, G.; Baccile, N. PH-Triggered Formation of Nanoribbons from Yeast-Derived Glycolipid Biosurfactants. *Soft Matter* **2014**, *10*,

3950–3959.

(56) Liu, W.; Sun, S.; Cao, Z.; Zhang, X.; Yao, K.; Lu, W. W.; Luk, K. D. K. An Investigation on the Physicochemical Properties of Chitosan/DNA Polyelectrolyte Complexes. *Biomaterials* **2005**, *26*, 2705–2711.

(57) Lewis, S. R.; Datta, S.; Gui, M.; Coker, E. L.; Huggins, F. E.; Daunert, S.; Bachas, L.; Bhattacharyya, D. Reactive Nanostructured Membranes for Water Purification. *Proc. Natl. Acad. Sci. U. S. A.* **2011**, *108*, 8577–8582.

(58) Mady, M. M.; Mohammed, W. A.; El-Guendy, N. M.; Elsayed, A. A. Effect of Polymer Molecular Weight on the Dna/Pei Polyplexes Properties. *J. Biophys* **2011**, *21*, 151–165.

(59) Ben Messaoud, G.; Le Griel, P.; Hermida-Merino, D.; Roelants, S. L. K. W.; Soetaert, W.; Stevens, C. V.; Baccile, N. PH-Controlled Self-Assembled Fibrillar Network (SAFiN) Hydrogels: Evidence of a Kinetic Control of the Mechanical Properties. *Chem. Mater.* **2019**, *31*, 4817–4830.

(60) Schindelin, J.; Arganda-Carreras, I.; Frise, E.; Kaynig, V.; Longair, M.; Pietzsch, T.; Preibisch, S.; Rueden, C.; Saalfeld, S.; Schmid, B.; et al. Fiji: An Open-Source Platform for Biological-Image Analysis. *Nat. Methods* **2012**, *9*, 676–682.

(61) Koga, S.; Williams, D. S.; Perriman, A. W.; Mann, S. Peptide-Nucleotide Microdroplets as a Step towards a Membrane-Free Protocell Model. *Nat. Chem.* **2011**, *3*, 720–724.

(62) Swanson-Vethamuthu, M.; Dubin, P. L.; Almgren, M.; Yingjie, L. Cryo-TEM of Polyelectrolyte – Micelle Complexes. *J. Colloid Interface Sci.* **1997**, *186*, 414–419.

(63) Rinaudo, M. Chitin and Chitosan: Properties and Applications. *Prog. Polym. Sci.* **2006**, *31*, 603–632.

(64) Seyrig, C.; Griel, P. Le; Cowieson, N.; Perez, J.; Baccile, N. Synthesis of Multilamellar Walls Vesicles Polyelectrolyte-Surfactant Complexes from PH-Stimulated Phase Transition Using Microbial Biosurfactants. *J. Colloid Interface Sci.* **2020**, 10.1016/j.jcis.2020.07.021.

(65) Xu, A. Y.; Melton, L. D.; Ryan, T. M.; Mata, J. P.; Rekas, A.; Williams, M. A. K.; McGillivray, D. J. Effects of Polysaccharide Charge Pattern on the Microstructures of β-Lactoglobulin-Pectin Complex Coacervates, Studied by SAXS and SANS. *Food Hydrocoll.* **2018**, *77*, 952–963.

(66) Kronberg, B.; Holmberg, K.; Lindman, B. Surfactant–Polymer Systems. In *Surface Chemistry of Surfactants and Polymers*; Kronberg, B., Holmberg, K., Lindman, B.,

Eds.; John Wiley & Sons, Ltd., 2014; pp 271–294.

(67) Dias, R. S.; Dawson, K.; Miguel, M. G. Interaction of DNA with Surfactants in Solution. In *DNA Interactions with Polymers and Surfactants*; Dias, R., Lindman, B., Eds.; Hoboken, New Jersey, 2008; pp 89–117.

(68) Chiappisi, L.; David Leach, S.; Gradzielski, M. Precipitating Polyelectrolyte-Surfactant Systems by Admixing a Nonionic Surfactant-a Case of Cononsurfactancy. *Soft Matter* **2017**, *13*, 4988–4996.

(69) Israelachvili, J. N.; Mitchell, D. J. A Model for the Packing of Lipids in Bilayer Membranes. *Biochim. Biophys. Acta* **1975**, *389*, 13–19.

(70) Tanford, C. *The Hydrophobic Effect: Formation of Micelles and Biological Membranes*; Wiley-Interscience, 1973.

(71) Nagarajan, R. Self-Assembly of Bola Amphiphiles. *Chem. Eng. Commun.* **1987**, *55*, 251–273.

(72) Manet, S.; Cuvier, A. S.; Valotteau, C.; Fadda, G. C.; Perez, J.; Karakas, E.; Abel, S.; Baccile, N. Structure of Bolaamphiphile Sophorolipid Micelles Characterized with SAXS, SANS, and MD Simulations. *J. Phys. Chem. B* **2015**, *119*, 13113–13133.

(73) Borukhov, I.; Andelman, D.; Orland, H. Polyelectrolyte Solutions between Charged Surfaces. *Europhys. Lett.* **1995**, *32*, 499–504.

(74) Dobrynin, A. V.; Rubinstein, M. Theory of Polyelectrolytes in Solutions and at Surfaces. *Prog. Polym. Sci.* **2005**, *30*, 1049–1118.

(75) Dan, N.; Pincus, P.; Safran, S. A. Membrane-Induced Interactions between Inclusions. *Langmuir* **1993**, *9*, 2768–2771.

(76) Winterhalter, M.; Helfrich, W. Effect of Surface Charge on the Curvature Elasticity of Membranes. *J. Phys. Chem* **1988**, *92*, 6865–6867.

(77) Zinchenko, A. A.; Pyshkina, O. A.; Lezov, A. V.; Sergeyev, V. G.; Yoshikawa, K. Single DNA Molecules: Compaction and Decompaction. In *DNA Interactions with Polymers and Surfactants*; Dias, R., Lindman, B., Eds.; John Wiley & Sons, Inc.: Hoboken, New Jersey, 2008; pp 59–88.

(78) He, T. Estimating Cross-sectional Area of a Polymer Chain by Additive Method. *J. Appl. Polym. Sci.* **1986**, *31*, 1521–1524.

(79) Heath, G. R.; Li, M.; Polignano, I. L.; Richens, J. L.; Catucci, G.; O'Shea, P.; Sadeghi, S. J.; Gilardi, G.; Butt, J. N.; Jeuken, L. J. C. Layer-by-Layer Assembly of Supported Lipid Bilayer Poly-l-Lysine Multilayers. *Biomacromolecules* **2016**, *17*, 324–335.

(80) Netrabukkana, R.; Lourvanij, K.; Rorrer, G. L. Diffusion of Glucose and Glucitol in

Microporous and Mesoporous Silicate/Aluminosilicate Catalysts. *Ind. Eng. Chem. Res.* **1996**, *35*, 458–464.

(81) Parsegian, V. A.; Zemb, T. Hydration Forces: Observations, Explanations, Expectations, Questions. *Curr. Opin. Colloid Interface Sci.* **2011**, *16*, 618–624.

(82) Leikin, S.; Parsegian, V. A.; Rau, D. C.; Rand, R. P. Hydration Forces. *Annu. Rev. Phys. Chem.* **1993**, *44*, 369–395.

(83) Dubois, M.; Zemb, T.; Fuller, N.; Rand, R. P.; Parsegian, V. A. Equation of State of a Charged Bilayer System: Measure of the Entropy of the Lamellar-Lamellar Transition in DDABr. *J. Chem. Phys.* **1998**, *108*, 7855–7869.

(84) Ricoul, F.; Dubois, M.; Belloni, L.; Zemb, T.; André-Barrès, C.; Rico-Lattes, I. Phase Equilibria and Equation of State of a Mixed Cationic Surfactant-Glycolipid Lamellar System. *Langmuir* **1998**, *14*, 2645–2655.

(85) Leneveu, D. M.; Rand, R. P.; Parsegian, V. A. Measurement of Forces between Lecithin Bilayers. *Nature* **1976**, *259*, 601–603.

(86) Claesson, P. M. Interactions Between Surfaces Coated with Carbohydrates, Glycolipids, and Glycoproteins. In *Biopolymers at Interfaces, Second Edition*; Malmsten, M., Ed.; CRC Press, 2003; p 165.

(87) Chatellier, X.; Joanny, J.-F. Adsorption of Polyelectrolyte Solutions on Surfaces: A Debye-Hueckel Theory. *J. Phys. II Fr.* **1996**, *6*, 1669–1686.

(88) Yethiraj, A. Forces between Surfaces Immersed in Polyelectrolyte Solutions. *J. Chem. Phys.* **1999**, *111*, 1797–1800.

(89) Dobrynin, A. V.; Deshkovski, A.; Rubinstein, M. Adsorption of Polyelectrolytes on Oppositely Charged Surfaces. *Macromolecules* **2001**, *34*, 3421–3436.

(90) Rand, R. P.; Parsegian, V. A. Hydration Forces between Phospholipid Bilayers. *BBA - Rev. Biomembr.* **1989**, *988*, 351–376.

(91) Kanicky, J. R.; Shah, D. O. Effect of Degree, Type, and Position of Unsaturation on the PKa of Long-Chain Fatty Acids. *J. Colloid Interface Sci.* **2002**, *256*, 201–207.

(92) Lieckfeldt, R.; Villalaín, J.; Gómez-Fernández, J.-C.; Lee, G. Apparent Pka of the Fatty Acids Within Ordered Mixtures of Model Human Stratum Corneum Lipids. *Pharm. Res.* **1995**, *12*, 1614–1617.

(93) Satake, I.; Yang, J. T. Interaction of Sodium Decyl Sulfate with Poly(L-ornithine) and Poly(L-lysine) in Aqueous Solution. *Biopolymers* **1976**, *15*, 2263–2275.

(94) Nishio, T.; Shimizu, T.; Kwak, J. C. T.; Minakata, A. The Cooperative Binding of Large Ligands to a One-Dimensional Lattice: The Steric Hindrance Effect. *Biophys.*

Chem. **2003**, *104*, 501–508.

(95) Nishio, T.; Shimizu, T. Model Analysis of Surfactant-Polymer Interaction as Cooperative Ligand Binding to Linear Lattice. *Biophys. Chem.* **2005**, *117*, 19–25.

(96) Instruments, T. Microcalorimetry Introduction to Characterizing Biopolymer Binding and Kinetics Reactions by ITC. **2009**, 1–42.

(97) Aberkane, L.; Jasniewski, J.; Gaiani, C.; Scher, J.; Sanchez, C. Thermodynamic Characterization of Acacia Gum-β-Lactoglobulin Complex Coacervation. *Langmuir* **2010**, *26*, 12523–12533.

(98) Kayitmazer, A. B. Thermodynamics of Complex Coacervation. *Adv. Colloid Interface Sci.* **2017**, *239*, 169–177.

(99) Freire, E.; Mayorga, O. L.; Straume, M. Isothermal Titration. *Anal. Chem.* **1990**, *62*, 950A-959A.

(100) van Holde, K. E. No Title. In *Physical Biochemistry, 2nd éd.; Prentice-Hall: Englewood Cliffs, NJ,*; 1985; p chapter 3.

(101) Cantor, C. R.; Schimmel, P. R. No Title. In *Cantor, C. R.; Schimmel, P. R. Biophysical Chemistry, Part III: The Behavior of Biological Macromolecules; W. H. Freeman: New York*; 1980; p chapter 15.

(102) Harnsilawat, T.; Pongsawatmanit, R.; McClements, D. J. Characterization of β-Lactoglobulin-Sodium Alginate Interactions in Aqueous Solutions: A Calorimetry, Light Scattering, Electrophoretic Mobility and Solubility Study. *Food Hydrocoll.* **2006**, *20*, 577–585.

(103) Du, X.; Dubin, P. L.; Hoagland, D. A.; Sun, L. Protein-Selective Coacervation with Hyaluronic Acid. *Biomacromolecules* **2014**, *15*, 726–734.

(104) Priftis, D.; Laugel, N.; Tirrell, M. Thermodynamic Characterization of Polypeptide Complex Coacervation. *Langmuir* **2012**, *28*, 15947–15957.

(105) Yu, S.; Xu, X.; Yigit, C.; Van Der Giet, M.; Zidek, W.; Jankowski, J.; Dzubiella, J.; Ballauff, M. Interaction of Human Serum Albumin with Short Polyelectrolytes: A Study by Calorimetry and Computer Simulations. *Soft Matter* **2015**, *11*, 4630–4639.

(106) Krouská, J.; Pekař, M.; Klučáková, M.; Šarac, B.; Bešter-Rogač, M. Study of Interactions between Hyaluronan and Cationic Surfactants by Means of Calorimetry, Turbidimetry, Potentiometry and Conductometry. *Carbohydr. Polym.* **2017**, *157*, 1837–1843.

(107) Vinayahan, T.; Williams, P. A.; Phillips, G. O. Electrostatic Interaction and Complex Formation between Gum Arabic and Bovine Serum Albumin. *Biomacromolecules*

2010, *11*, 3367–3374.

(108) Dubin, P. L.; Gruber, J. H.; Xia, J.; Zhang, H. The Effect of Cations on the Interaction between Dodecylsulfate Micelles and Poly(Ethyleneoxide). *J. Colloid Interface Sci.* **1992**, *148*, 35–41.

(109) Marques, E. F.; Regev, O.; Khan, A.; Miguel, M. D. G.; Lindman, B. Interactions between Catanionic Vesicles and Oppositely Charged Polyelectrolytes - Phase Behavior and Phase Structure. *Macromolecules* **1999**, *32*, 6626–6637.

(110) De Souza, T. P.; Bossa, G. V.; Stano, P.; Steiniger, F.; May, S.; Luisi, P. L.; Fahr, A. Vesicle Aggregates as a Model for Primitive Cellular Assemblies. *Phys. Chem. Chem. Phys.* **2017**, *19*, 20082–20092.

(111) Weisman, S.; Hirsch-Lerner, D.; Barenholz, Y.; Talmon, Y. Nanostructure of Cationic Lipid-Oligonucleotide Complexes. *Biophys. J.* **2004**, *87*, 609–614.

(112) Ram-On, M.; Cohen, Y.; Talmon, Y. Effect of Polyelectrolyte Stiffness and Solution PH on the Nanostructure of Complexes Formed by Cationic Amphiphiles and Negatively Charged Polyelectrolytes. *J. Phys. Chem. B* **2016**, *120*, 5907–5915.

(113) Gasperini, A. A. M.; Puentes-Martinez, X. E.; Balbino, T. A.; De Paula Rigoletto, T.; De Sá Cavalcanti Corrêa, G.; Cassago, A.; Portugal, R. V.; De La Torre, L. G.; Cavalcanti, L. P. Association between Cationic Liposomes and Low Molecular Weight Hyaluronic Acid. *Langmuir* **2015**, *31*, 3308–3317.

Published in Langmuir DOI: 10.1021/acs.langmuir.0c01177

Supporting Information

Stimuli-induced non-equilibrium phase transitions in polyelectrolyte-surfactant complex coacervates

Chloé Seyrig,[a] Gertrude Kignelman,[b] Wim Thielemans,[b] Patrick Le Griel,[a] Nathan Cowieson,[c] Javier Perez,[d] Niki Baccile[a,*]

[a] Sorbonne Université, Centre National de la Recherche Scientifique, Laboratoire de Chimie de la Matière Condensée de Paris , LCMCP, F-75005 Paris, France

[b] Sustainable Materials Lab, Department of Chemical Engineering, KU Leuven, campus Kulak Kortrijk, Etienne Sabbelaan 53, 8500 Kortrijk, Belgium

[c] Diamond Light Source Ltd, Harwell Science and Innovation Campus, Didcot, OX11 0QX, U.K.

[d] SWING, Synchrotron Soleil, BP 48, 91192 Gif-sur-Yvette, France

* Corresponding author: niki.baccile@sorbonne-universite.fr

Content:

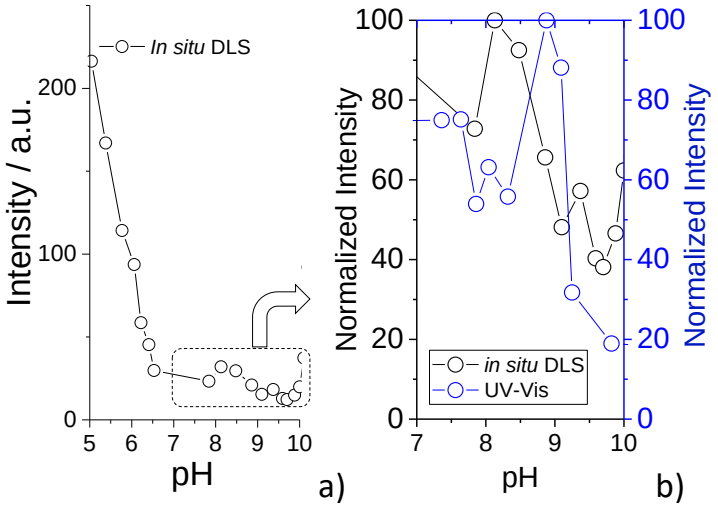

Figure S 1 – a) pH-resolved *in situ* turbidimetric experiment (DLS apparatus) performed on a [SL-C18:0 + PLL] solution at $C_{SL\text{-}C18:0}$= 2.5 mg·mL^{-1} C_{PLL}= 2.5 mg·mL^{-1}. b)-panel shows the normalized intensity recorded in turbidimetry experiments using the pH-resolved *in situ* DLS and UV-Vis apparatus.

To avoid sedimentation issues in the SL-C18:0 fibrillar system, we have repeated the turbidimetric titration of the [SL-C18:0 + PLL] mixture using a continuous flow-through device installed on a light scattering instrument and which guarantees a better homogenization of the sample solution. Data in Figure S 1 show a scattering behavior, in which one can identify some scattering above pH 10, due to the formation of platelets in the SL-C18:0 system alone,[1] and a strong scattering below pH 7, as reported elsewhere for the SL-C18:0 system alone.[2] Interestingly, the region between pH 7 and 10 is characterized by a mild scattering but comparable, after normalization, to the scattering observed in UV-Vis experiments (Figure S 1b). Whichever the method of analysis employed, we systematically find a region of pH, generally between 7 and 10, in which the lipid-PEC mixed solution becomes turbid, differently than the controls.

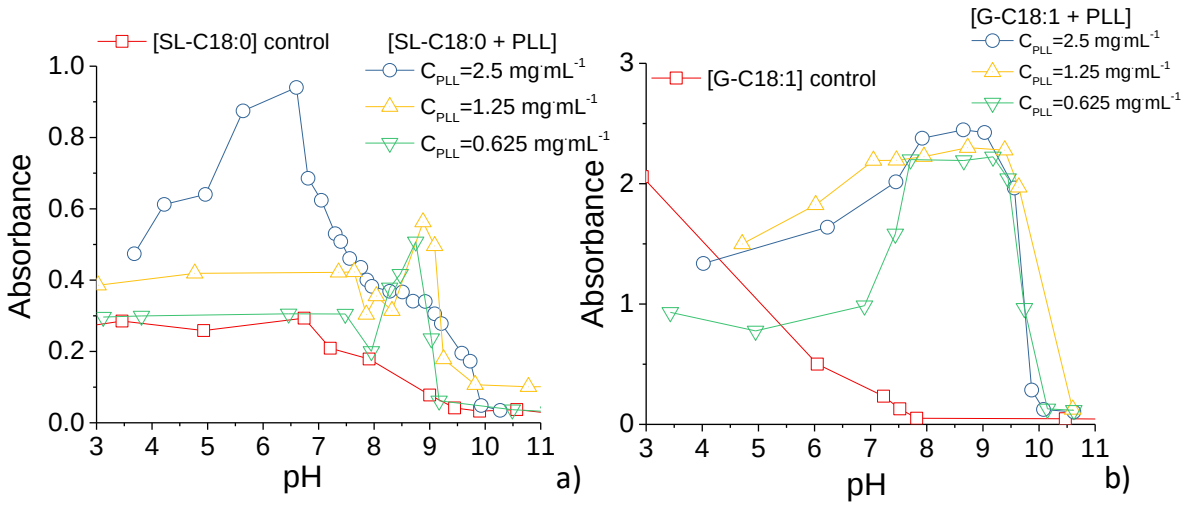

Figure S 2 - Room temperature turbidimetric analysis of a) SL-C18:0 and b) G-C18:1 glycolipid solutions with different concentrations of PLL as a function of pH. The typical sample preparation is described in the materials and method section. The final lipid and PLL concentrations are $C_{G\text{-}C18:1}$= $C_{SL\text{-}C18:0}$= 2.5 mg·mL^{-1}, C_{PLL}= 2.5, 1.25 or 0.625 mg·mL^{-1}. pH is decreased from 11 to 3.

The red square curve Figure S 2 refers to the control lipid solutions, displaying a similar behavior: the micellar region at alkaline pH shows poor scattering, while the intensity increases at acidic pH, when SL-C18:0 and G-C18:1 respectively self-assemble into fibers and vesicles. When mixed with different concentrations of PLL, all scattering profiles show a common bell-like shape, with an enhanced signal between pH 7 and 10. Indeed, blue, yellow and green curves, respectively standing for concentration of PLL of 2.5 mg.mL^{-1}, 1.25 mg.mL^{-1} and 0.625 mg.mL^{-1}, show an intensity peak at around pH 8.5 - 9. This behavior clearly identifies a preferred pH range of interaction between lipids and PLL, precisely from pH 7 to pH 9.

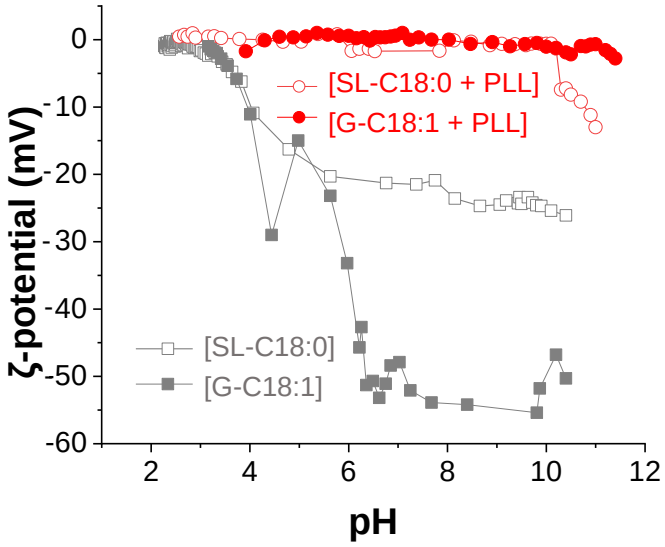

Figure S 3 – ζ-potential measurements of: [SL-C18:0] and [G-C18:1] controls (grey curves); [SL-C18:0 + PLL] and [G-C18:1 + PLL] solutions (red curves) $C_{G\text{-}C18:1} = C_{SL\text{-}C18:0} = 2.5$ **mg·mL^{-1},** $C_{PLL} = 2.5$ **mg·mL^{-1}**

ζ-potential experiments shown in Figure S 3 show that control lipid solutions have the same behavior: they are strongly negative (SL-C18:0 and G-C18:1 respectively show a plateau at -20 mV and -55 mV) under alkaline conditions, but their ζ-potentials slightly increase around pH 6 to finally be close to zero, putting in evidence the neutralization of the carboxylate group. When lipids are mixed with PLL, the resulting curve oscillates around neutral ζ-potential, and charges are perfectly compensated in the pH region of interest, from pH 7 to 9, an argument in favor of coacervation, a process likely occurring in electroneutralization conditions [3]

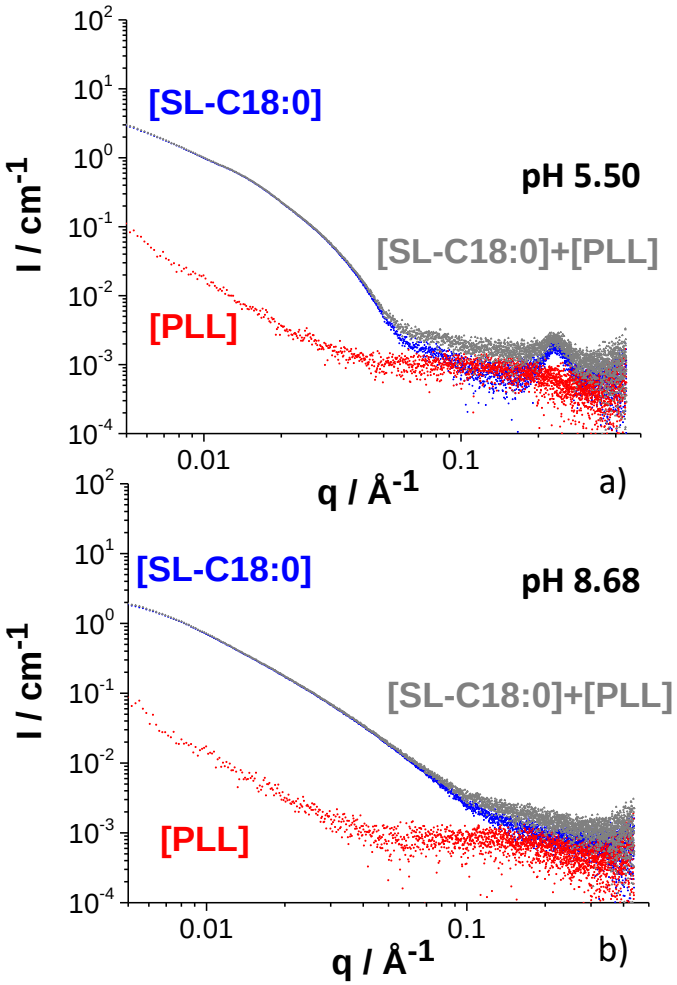

Figure S 4 - SAXS profiles of [SL-C18:0] and [PLL] controls at acidic and basic pH. $C_{SL\text{-}C18:0}$= 2.5 mg·mL^{-1}, C_{PLL}= 2.5 mg·mL^{-1}. [SL-C18:0] + [PLL] refers to the arithmetic sum of individual [SL-C18:0] and [PLL] signals.

Figure S 4 shows the control signals of single components: the red curve for [PLL] alone and the blue one for [SL-C18:0] alone. The grey curve corresponds to the simple arithmetic sum of both signals.

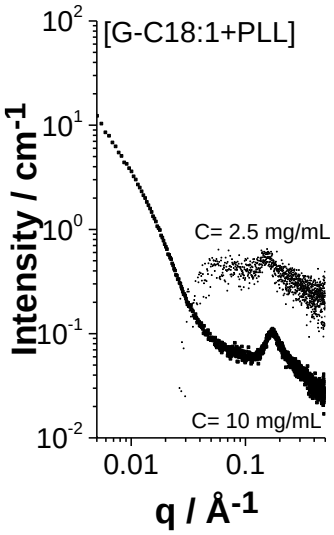

Figure S 5 - SAXS profiles of [G-C18:1 + PLL] solutions at two concentrations ($C_{G\text{-}C18:1}$= C_{PLL}) and pH 8.

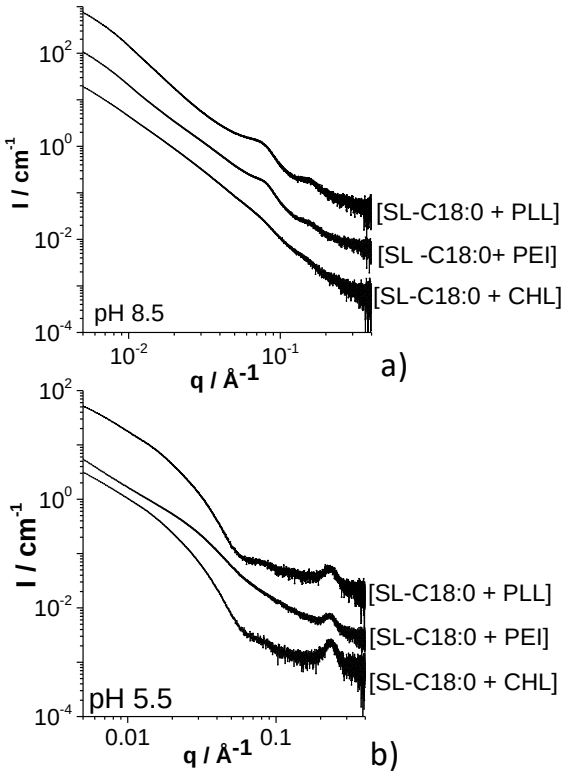

Figure S 6 - SAXS profiles of SL-C18:0 mixed with different polyelectrolytes at acidic and basic pH. $C_{SL\text{-}C18:0} = C_{PLL} = C_{PEI} = C_{CHL} = 2.5\ mg{\cdot}mL^{-1}$

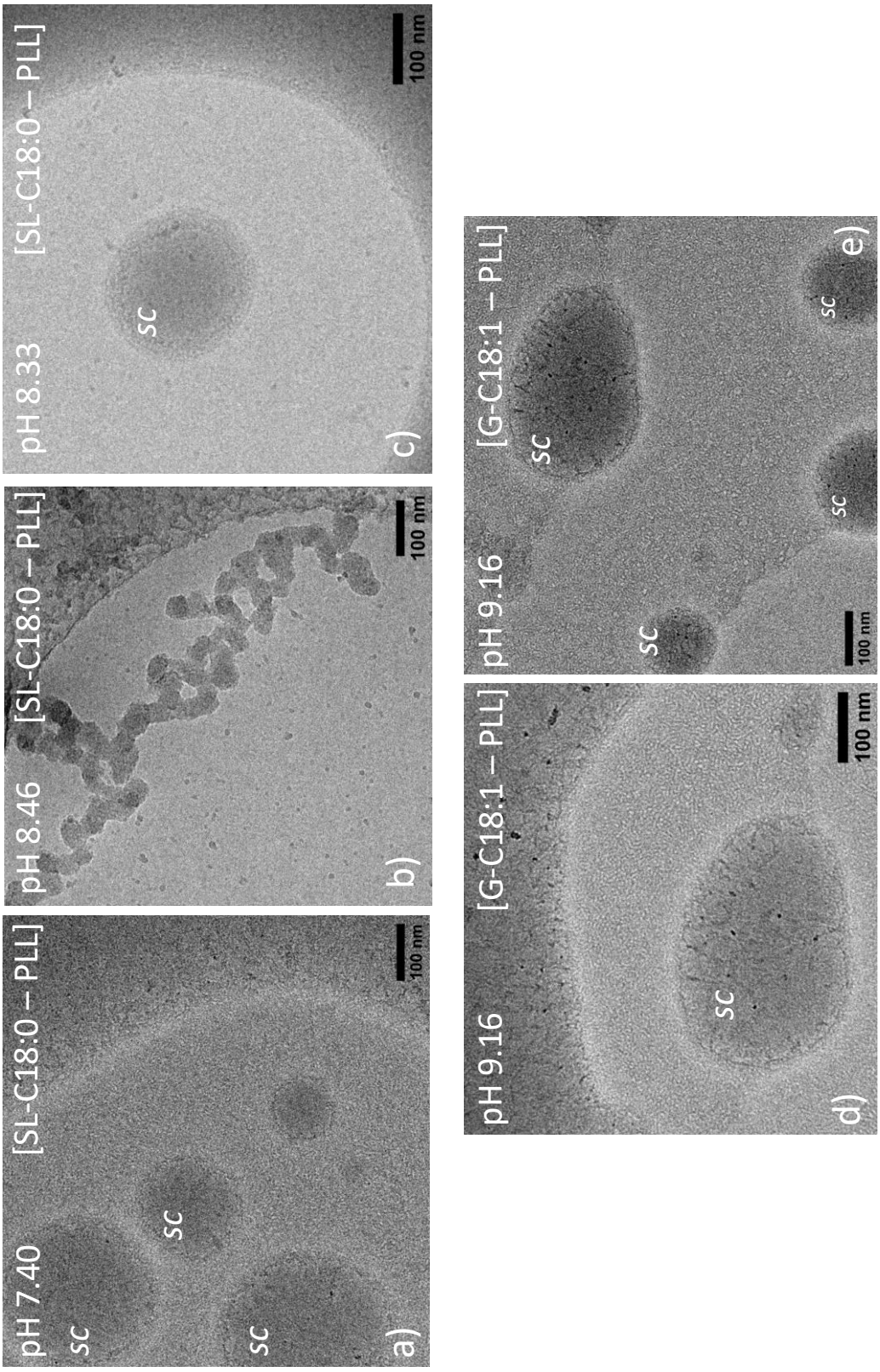

Figure S 7 - Cryo-TEM images of [SL-C18:0 + PLL] and [G-C18:1 + PLL] complex coacervates recorded at various pH values. $C_{SL\text{-}C18:0}$**=** $C_{G\text{-}C18:1}$ **=2.5 mg·mL^{-1};** C_{PLL}**= = 1.25 mg·mL^{-1}.** ***sc*** **stands for spherical colloid.**

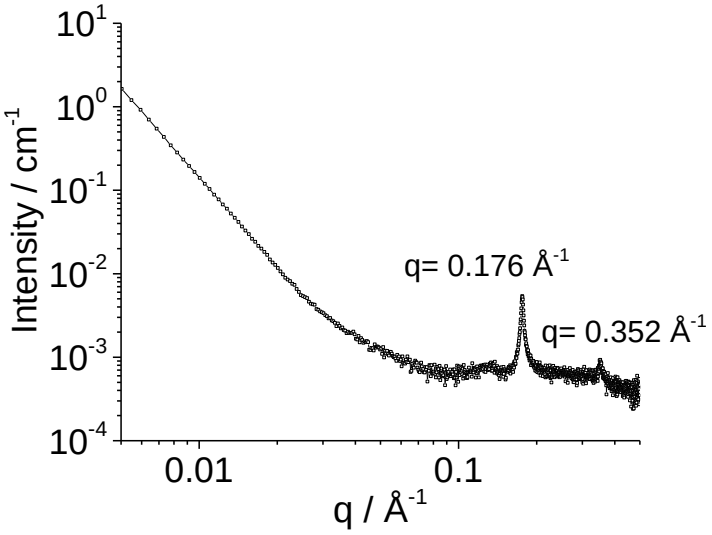

Figure S 8 - SAXS plots of the G-C18:1 control solution at *C*= 2.5 mg·mL^{-1} and pH 3. Experiment extracted from 2D contour plot in Figure 5a in the main text.

Published in Langmuir DOI: 10.1021/acs.langmuir.0c01177

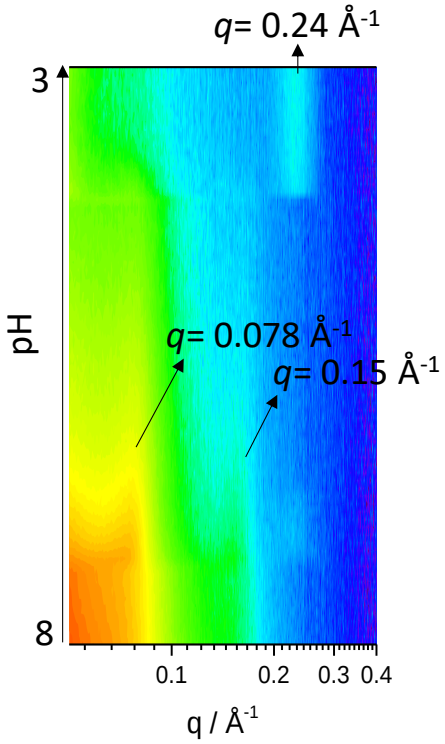

Figure S 9 - pH-resolved *in situ* SAXS 2D contour plot of the [SL-C18:0 + PLL] solution at $C_{SL\text{-}C18:0}$= C_{PLL}= 2.5 mg·mL^{-1}. Highlight of the coacervate-to-fiber transition between pH 8 and 3.

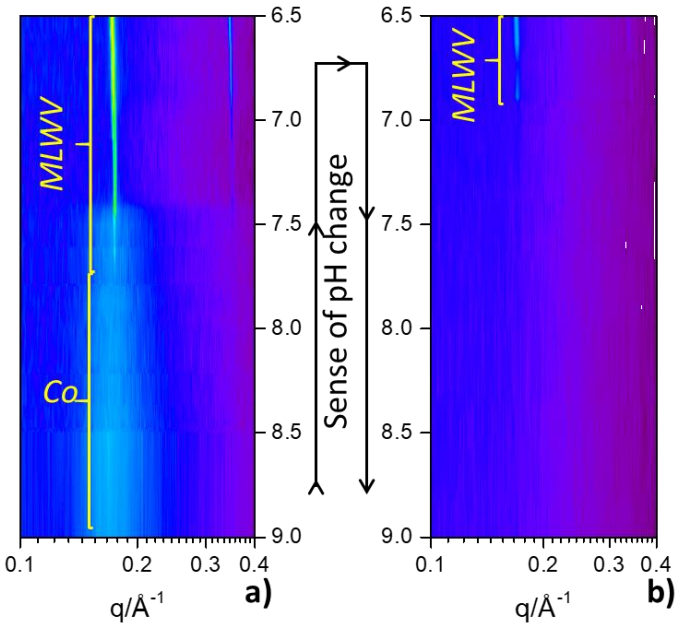

Figure S 10 - pH-resolved *in situ* SAXS 2D contour plots of the [G-C18:1 + PLL] solutions at $C_{G\text{-}C18:1}$= C_{PLL}= 2.5 mg·mL^{-1}: highlight of the *Co*-to-*MLWV* transition between pH 9 and 6.5. In a), pH is reduced from 10 to 3. Contour plot in b) is recorded on the same sample as in a), to which pH is increased from 3 to 10.

Published in Langmuir DOI: 10.1021/acs.langmuir.0c01177

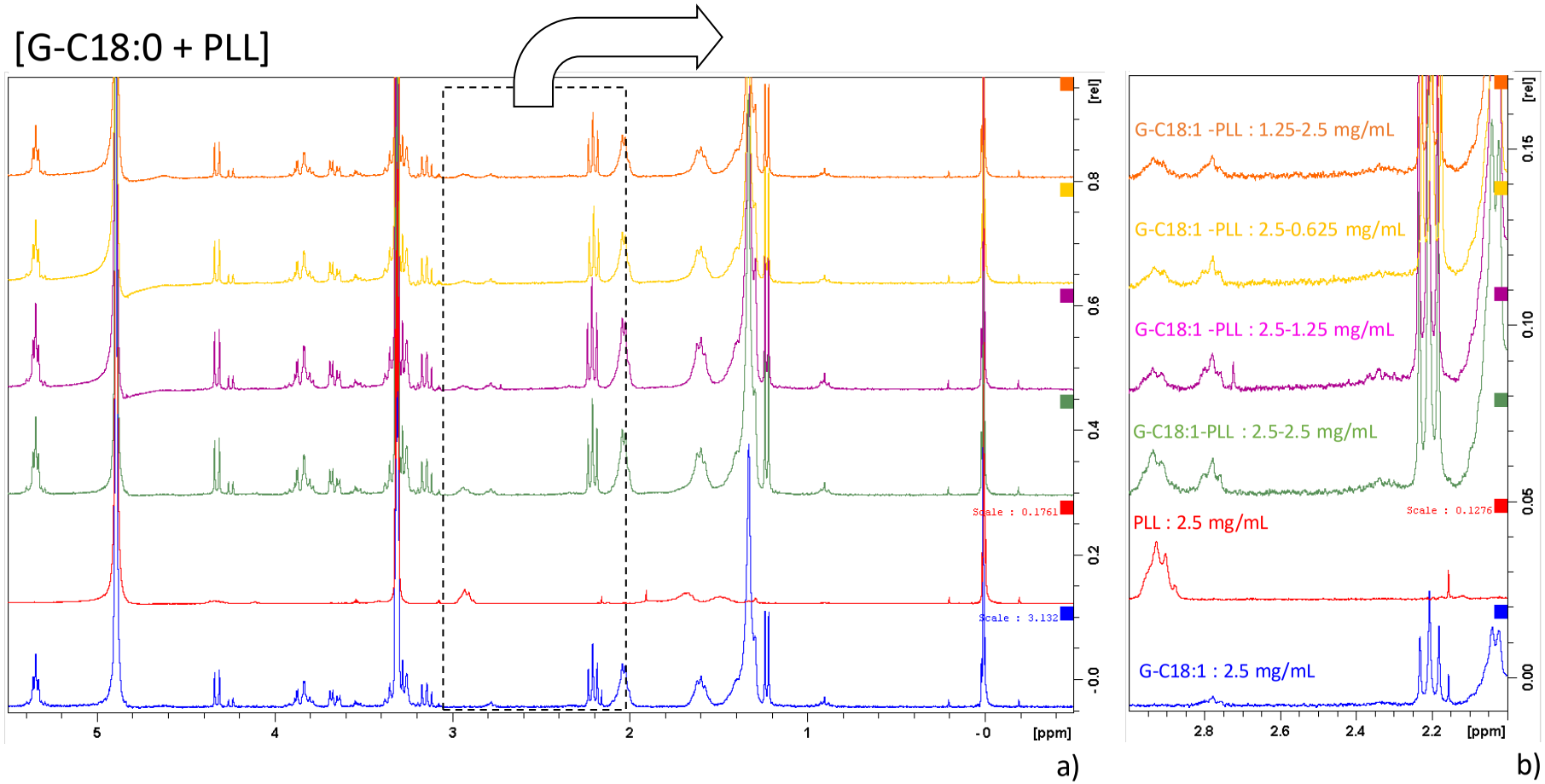

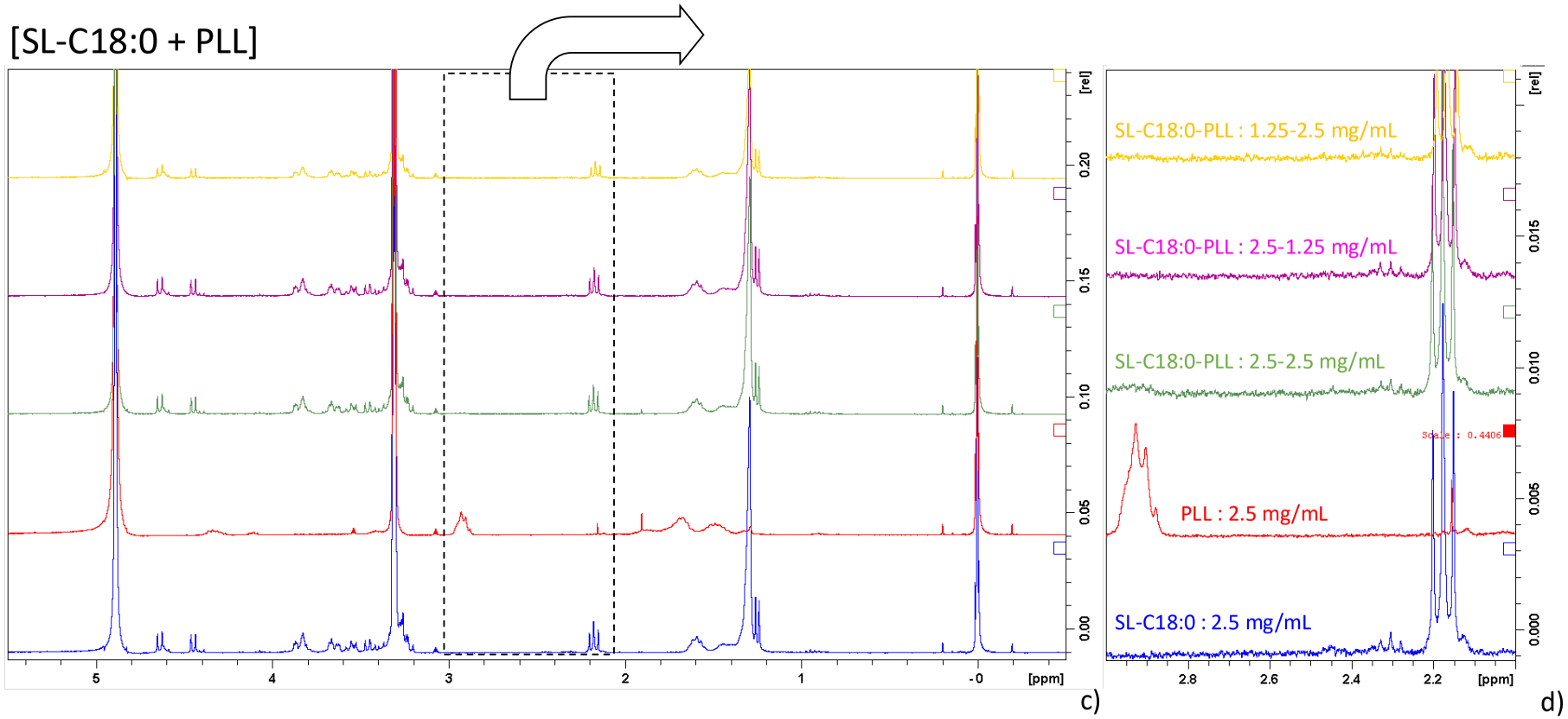

Figure S 11 – ^{1}H NMR spectra of a,b) G-C18:1, PLL, [G-C18 :0 + PLL] and c,d) SL-C18:0, PLL, [SL-C18 :0 + PLL] samples in MeOD-d4 (V= 500 µL) and corresponding zoom (b, d) of the 3.0 < δ / ppm < 2.0 region. Concentrations given next to each [SL-C18 :0 + PLL] spectrum refer to the initial concentration of each component in water at pH 5. Under these conditions, [SL-C18 :0 + PLL] form fibers while [G-C18:1 + PLL] forms *MLWV*. Both fibers and *MLWV* are centrifuged out of the parent solution, dried at 40°C during two days and dispersed in 500 µL MeOD-d4 for NMR analysis.

Table S 1 – Quantitative analysis of the integrals corresponding to the ^{1}H NMR spectra of the [G-C18:1 +PLL] samples in MeOD-d4, shown in Figure S 11. PLL is represented by the ($RC\underline{H_2}NH_2)_x$ (x ~ 20) peak at δ= 2.92 ppm. The M_w (PLL)≈ 1-5 KDa, we then consider an average M_w (PLL)= 2.5 kDa, whereas the M_w of each monomer is 128 g/mol, yielding an average of 20 monomers per PLL chain. The valence of the ($RC\underline{H_2}NH_2)_x$ (x ~ 20) peak is then taken as 40. G-C18:1 is represented by the $RC\underline{H_2}C{=}O$ peak at δ= 2.2 ppm. The M_w (G-C18:1)= 460 g/mol and each G-C18:1 bears a single COOH group. The valence of the $RC\underline{H_2}C{=}O$ peak is then taken as 2. The peak at δ= 0 ppm corresponds to the reference (TMSP-d4, 1 mg.mL^{-1}≡ 5.8 mM), having a valence of 9.

Explanation of columns: C_{In} represents the nominal concentration of G-C18:1 and PLL in 1 mL water at pH 5; the Integrals column provides the values of the integrals of G-C18:1, PLL and TMSP-d4 normalized to the valence of each peak and collected on centrifuged MLWV dispersed in 500 µL MeOD-d4; C_F represents the concentration of G-C18:1 and PLL in MLWV calculated from their respective integrals with respect to TMSP-d4 ($I_{average\ @\ 0\ ppm}$/9= 9708296 ± 120685) for an equivalent 1 mL of solution. $\frac{C_F}{C_I}$ represents the amount (%) of G-C18:1 and PLL consumed in the formation of MLWV. The Molar ratio column gives the G-C18:1-to-PLL molar ration in the initial solution and in the MLWV. $\frac{[COOH]_F}{[NH_2]_F}$ represents the G-C18:1-to-PLL monomer molar ratio in MLWV. All errors are calculated from the propagation of errors in respect of the integral of the reference.

C_{In}		Integrals			C_F		$\frac{C_F}{C_{In}}$		Molar ratio		Functional group ratio in MLWV
$[G-C18:1]_{In}$ mM (mg.mL^{-1})	$[PLL]_{In}$ mM (mg.mL^{-1})	G-C18:1	PLL	TMSP-d4	$[G-C18:1]_F$ mM	$[PLL]_F$ x 10^{-2} mM	$\frac{[G-C18:1]_F}{[G-C18:1]_{In}}$ %	$\frac{[PLL]_F}{[PLL]_{In}}$ %	$\frac{[G-C18:1]_{In}}{[PLL]_{In}}$ *(in solution)*	$\frac{[G-C18:1]_F}{[PLL]_F}$ *(in MLWV)*	$\frac{[COOH]_F}{[NH_2]_F}$
		$I_{2.2\ ppm}/2$	$I_{2.8\ ppm}/40$	$I_{0\ ppm}/9$							
5.4 (2.5)	1 (2.5)	11320838	122969	9725633	3.4 ± 0.6	3.7 ± 0.6	63 ± 11	3.7 ± 0.6	5.4	92 ± 22	4.6 ± 1.1
5.4 (2.5)	0.5 (1.25)	12427299	64857	9728182	3.7 ± 0.6	1.9 ± 0.3	69 ± 12	3.9 ± 0.7	10.8	192 ± 46	9.6 ± 2.3
5.4 (2.5)	0.25 (0.625)	8480098	58866	9835125	2.5 ± 0.4	1.8 ± 0.3	47 ± 8	7.0 ± 1.2	21.6	144 ± 35	7.2 ± 1.7
2.75 (1.25)	1 (2.5)	8687840	76772	9544245	2.6 ± 0.4	2.3 ± 0.4	94 ± 16	2.3 ± 0.4	2.75	113 ± 27	5.7 ± 1.4

Table S 2 - ITC experiments: parameters extracted from the "multiple sites" model fit of G-C18:1 4 mM into PLL 2 mM data after subtracting the buffer contribution.

Interaction type	Parameter	Value
Non-specific Endothermic (entropic, hydrophobic effect)	K_{a1}	$3.2 \cdot 10^8$ M^{-1}
	n_1	0.05
	ΔG_1	-48.6 kJ/mol
	ΔH_1	5.3 kJ/mol
	ΔS_1	0.18 kJ/mol·K
Specific Exothermic (electrostatic, H-bonding)	K_{a2}	$1.1 \cdot 10^6$ M^{-1}
	n_2	4.3
	ΔG_2	-34.6
	ΔH_2	-2.0 kJ/mol
	ΔS_2	0.11 kJ/mol·K

Table S 3 - ITC experiments: parameters extracted from the "multiple sites" model fit of G-C18:1 2 mM into PLL 2 mM data after subtracting the buffer contribution.

Interaction type	Parameter	Value
Non-specific Endothermic (entropic, hydrophobic effect)	K_{a1}	$1.7 \cdot 10^8$ M^{-1}
	n_1	0.01
	ΔG_1	-46.8 kJ/mol
	ΔH_1	52.6 kJ/mol
	ΔS_1	0.33 kJ/mol·K
Specific Exothermic (electrostatic, H-bonding)	K_{a2}	$4.1 \cdot 10^6 M^{-1}$
	n_2	3.3
	ΔG_2	-38.3
	ΔH_2	-3.6 kJ/mol
	ΔS_2	0.12 kJ/mol·K

References

(1) Cuvier, A. S.; Babonneau, F.; Berton, J.; Stevens, C. V.; Fadda, G. C.; Péhau-Arnaudet, G.; Le Griel, P.; Prévost, S.; Perez, J.; Baccile, N. Nanoscale Platelet Formation by Monounsaturated and Saturated Sophorolipids under Basic PH Conditions. *Chem. - A Eur. J.* **2015**, *21*, 19265–19277.

(2) Cuvier, A. S.; Berton, J.; Stevens, C. V.; Fadda, G. C.; Babonneau, F.; Van Bogaert, I. N. A.; Soetaert, W.; Pehau-Arnaudet, G.; Baccile, N. PH-Triggered Formation of Nanoribbons from Yeast-Derived Glycolipid Biosurfactants. *Soft Matter* **2014**, *10*, 3950–3959.

(3) Wang, Y.; Kimura, K.; Huang, Q.; Dubin, P. L. Effects of Salt on Poly Electrolyte-Micelle Coacervation. *Macromolecules* **1999**, *32*, 7128–7134.